To the Graduate Council:

I am submitting herewith a thesis written by Jeong Kwan Na entitled "Bragg Imaging of Light Diffracted by Ultrasonic Waves and Its Application to Flaw Detection." I have examined the final copy of this thesis for form and content and recommend that it be accepted in partial fulfillment of the requirements for the degree of Master of Science, with a major in Physics.

M. A. Breazeale, Major Professor

We have read this thesis and recommend its acceptance:

W. E. Reeds

Chas C. Slack

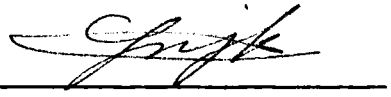
Accepted for the Council:

Vice Provost
and Dean of the Graduate School

STATEMENT OF PERMISSION TO USE

In presenting this thesis in partial fulfillment of the requirements for a Master's degree at The University of Tennessee, Knoxville, I agree that the Library shall make it available to borrowers under rules of the Library. Brief quotations from this thesis are allowable without special permission, provided that accurate acknowledgment of source is made.

Permission for extensive quotation from or reproduction of this thesis may be granted by my major professor, or in his absence, by the Head of Interlibrary Services when, in the opinion of either, the proposed use of the material is for scholarly purposes. Any copying or use of the material in this thesis for financial gain shall not be allowed without my written permission.

Signature 

Date 11/25/86

BRAGG IMAGING OF LIGHT DIFFRACTED BY ULTRASONIC WAVES AND ITS APPLICATION TO FLAW DETECTION

A Thesis

Presented for the

Master of Science

Degree

The University of Tennessee, Knoxville

Jeong Kwan Na

December 1986

ACKNOWLEDGMENTS

The author expresses his sincere gratitude to Dr. M. A. Breazeale, who patiently directed this research, for his suggestions, constant encouragement, and criticism. Special thanks must be given to Dr. O. Leroy for his discussions, insight, and assistance.

The author wishes to thank the Office of Naval Research for financial assistance and for the use of many facilities.

He thanks Maxine Martin for typing this thesis.

He is also grateful to his wife, Il Cheon, whose encouragement has made this work possible.

ABSTRACT

Diffraction of light by ultrasonic waves in water has been studied in the range of frequencies 4 MHz and 28 MHz. In the lower frequency of range Raman-Nath diffraction is observed. As the frequency increases the diffraction becomes more and more analogous to x-ray diffraction by crystalline lattices and hence is referred to as Bragg diffraction. In the Raman-Nath range diffraction is optimum at normal incidence. In the Bragg range diffraction is optimum for nonnormal incidence. For light incident at the angle of optimum Bragg diffraction images of the ultrasonic wavefront appear in the diffraction orders. One image is observed in the first orders and two images appear in the second orders. The theory of Blomme and Leroy (Acustica 59, 182-192, 1986) is used to analyze the Bragg diffraction. It is adequate to explain imaging in both the first and second orders.

A practical application to flaw detection is made by using Bragg diffraction to image irregularities inside parallel plates of metal or glass.

TABLE OF CONTENTS

CHAPTER		PAGE
I.	INTRODUCTION	1
II.	THEORETICAL CONSIDERATIONS	4
	Diffraction Theory of Raman and Nath	4
	Diffraction Theory of Klein, Cook, and Mayer	8
	Significance of Parameters	14
	Solutions of the Difference-Differential Equations for Raman and Nath Region ($Q << 1$)	17
	Diffraction Theory of Blomme and Leroy for the Bragg Region	19
III.	EXPERIMENTAL INVESTIGATION OF BRAGG IMAGING	26
	Apparatus	26
	Raman-Nath Diffraction System	26
	Bragg Diffraction Conditions	26
	Intensities of Diffraction Orders	28
	Bragg Diffraction System	31
	Experimental Observations	34
	First-Order Bragg Imaging	34
	Second-Order Bragg Imaging	36
IV.	ANALYSIS OF BRAGG IMAGING	40
	First-Order Bragg Imaging	42
	Second-Order Bragg Imaging	45
V.	APPLICATION OF BRAGG IMAGING TO FLAW DETECTING	49
VI.	SUMMARY, CONCLUSIONS, AND SUGGESTIONS FOR FURTHER WORK	56
	Summary and Conclusions	56
	Suggestions for Further Work	57
BIBLIOGRAPHY		59
VITA		61

LIST OF TABLES

TABLE		PAGE
I.	Comparison of Theoretical and Experimental Bragg Angles	29
II.	Angles at Which Optimum Bragg Diffraction is Observed With a Glass Plate 1.1 mm Thick, Frequency 12 MHz	53

LIST OF FIGURES

FIGURE		PAGE
1.	Diffraction Orders of Light Incident on an Ultrasonic Beam	7
2.	Diagram of the Ultrasonic Diffraction Grating	9
3.	Orientation of the Wave Vectors in Light Diffracted by an Ultrasonic Wave	12
4.	Light Intensities of Diffraction Orders Under Raman-Nath Conditions	20
5.	Experimental Arrangement for Raman-Nath Diffraction of Light by Ultrasonic Waves	27
6.	Intensities of Diffraction Orders Plotted as a Function of Raman-Nath Parameter v	30
7.	Experimental Arrangement of the Bragg Diffraction System	32
8.	Photograph of Experimental Arrangement of Bragg Diffraction System	33
9.	Photographs of Objects and Their First-Order Bragg Images: (a) Hook, Spring, and Nut; (b) Frequency 20 MHz and Width of Ultrasound 2.4 cm; (c) Frequency 10 MHz and Width of Ultrasound 4.8 cm	35
10.	Photographs of First-Order Bragg Images of Hook, Spring, and Nut, Frequency 28 MHz	37
11.	Photographs of Positive and Negative First-Order Bragg Images of a Hook, Frequency 20 MHz	38
12.	Photographs of First- and Second-Order Images of a Nut, Frequency 12 MHz	39
13.	Diagram Showing the Origin of Light Arriving at the Observed Diffraction Order	41
14.	Light Intensities Plotted as a Function of the Incident Angle of Light for v = 3.09 ($\mu_1 = 1.3 \times 10^{-5}$) and for (a) ρ = 1.03 (ν^* = 10 MHz and β = 5.45 min); (b) ρ = 1.48 (ν^* = 12 MHz and β = 6.54 min); (c) ρ = 2.31 (ν^* = 15 MHz and β = 8.18 min)	43

FIGURE PAGE

15. Light Intensity Plotted as a Function of the Incident Angle of Light for v = 1.43 and ρ = 17.48 (ν^* = 28 MHz and β = 15.27 min) 44

16. Light Intensities of the Observed First- and Second-Order Bragg Diffraction Corresponding to Figure 14(b) . . 46

17. Photograph of Experimental Arrangement for Flaw Detecting 50

18. Photographs of the Symbol Ψ on the Glass Plate and Its Image, Frequency 20 MHz 51

19. Photographs of the Symbol Ψ on the Aluminum Plate and Its Image, Frequency 20 MHz 54

20. Photographs of the Letters A and F Scratched on the Surface of an Aluminum Plate and Their Images 55

CHAPTER I

INTRODUCTION

A theory describing the diffraction of light by ultrasonic waves was developed in a series of papers by Raman and Nath (1935-36). Although their paper on the generalized theory of the interaction of light and ultrasound included equations applicable to Bragg diffraction, this fact was not generally recognized until Phariseau (1956) used their equations to calculate light intensities in the diffraction orders.

In the study of the diffraction of light by ultrasound, one distinguishes between "regular" diffraction and Bragg diffraction. "Regular" diffraction, usually referred to as Raman-Nath diffraction, is analogous to the diffraction of light by a ruled grating. Bragg diffraction of light by ultrasound is more analogous to the diffraction of x-rays by a crystalline lattice. Theoretical treatment of Raman-Nath diffraction can be made by considering the effect of variations in refractive index caused by the ultrasound. Bragg diffraction, however, is treated as if it were reflection of light by the individual wavefronts in a periodic perturbed medium. Thus Bragg diffraction theory is simply a treatment of the scattering of electromagnetic waves by a periodically perturbed medium.

Theoretical analysis of the region of overlap of Raman-Nath diffraction and Bragg diffraction has been greatly simplified by

Klein, Cook, and Mayer (1965, 1967) who defined a dimensionless parameter Q whose value allows one to determine which type of diffraction is dominant. Their Q parameter is used in this thesis to define the experimental conditions for optimum imaging.

A means of studying Bragg diffraction was developed by Korpel (1969) who demonstrated that the first Bragg diffraction order contains an image of the ultrasonic wavefront. He showed that objects placed in the ultrasonic beam were imaged in the first diffraction order. In order to explain these observations, he treated the Bragg diffraction process as analogous to parametric mixing and showed that there is a one-to-one mapping of the ultrasonic wavefront onto the first diffraction order.

The existence of multiple images in the higher order Bragg diffraction was first observed experimentally by Martin (1971). He extended Korpel's mapping theory of Bragg diffraction to analyze the existence of two images in the second diffraction order. His result, however, has proved to be inadequate. His mapping theory predicts that one point on the diffraction order is mapped from two different points on the ultrasonic wavefront. Although this may be true, it is inadequate to describe experimental results, as will be shown.

In this thesis experimental observations of the first- and second-order Bragg diffraction are reported. These observations are compared with theoretical predictions using the Nth Order Approximation (NOA) theory of Blomme and Leroy (1986) which is an approximation method to obtain analytical solution of the difference-differential equations describing Bragg diffraction.

Application of Bragg imaging to flaw detection also is reported. Both parallel glass plates and parallel aluminum plates are used. A flaw on (or in) the plates is imaged because a solid plate in a liquid medium transmits a maximum amount of the incident ultrasound at the angles at which Lamb modes are excited within the plates, but a smaller amount is transmitted at the flaw. The transmitted wavefront containing an image of the flaw is imaged in the Bragg diffraction order. Hence, Bragg diffraction can be used for flaw detection in parallel plates.

CHAPTER II

THEORETICAL CONSIDERATIONS

An understanding of the existence of Bragg imaging in the first diffraction order does not require a detailed theoretical discussion. As will be shown, the images and their origin are quite apparent. Bragg imaging in the second orders, however, is more complicated, and its origin can only be understood after the theory of Bragg diffraction is understood. For this reason it is worthwhile to begin with a discussion of Raman-Nath diffraction and show how the theoretical analysis changes as one increases the frequency of ultrasound and makes the transition to Bragg diffraction conditions.

I. DIFFRACTION THEORY OF RAMAN AND NATH

The diffraction of light by ultrasonic wave was treated by Raman and Nath (1935). Raman and Nath's diffraction theory is useful to understand Bragg diffraction. They stated that for a progressive periodic ultrasonic plane wave with light incident perpendicular to a sound beam, the light is diffracted at angles θ_n given by

$$n\lambda = \pm \lambda^* \sin \theta_n \qquad (1)$$

where n is an integer representing the diffraction orders, λ is the wavelength of the light, and λ^* is the wavelength of the sound.

Equation (1) was corrected by Klein, Cook, and Mayer (1965) to include the refractive index of the propagating medium:

$$n\lambda = \pm \mu_0 \lambda^* \sin \theta_n \ . \tag{2}$$

The refractive index μ_0 enters into Eq. (2) because the wavelength is given for free space and has to be adjusted for the particular medium used.

The intensity of the diffracted light in the m^{th} order relative to the n^{th} order is given by

$$\frac{I_m}{I_n} = \frac{J_m^2(v)}{J_n^2(v)} \tag{3}$$

where $J_m(v)$ and $J_n(v)$ are the m^{th} and n^{th} order Bessel function, respectively, and

$$v = 2\pi \mu_1 L/\lambda \ , \tag{4}$$

μ_1 is the maximum change of refractive index caused by the sound pressure, and L is the width of the sound field through which the light passes.

Raman and Nath (1935) extended this theory to the case of nonnormal incidence. If the light is incident at an angle on the ultrasonic wave, the relative intensity of the m^{th} order to the n^{th} order for low sound intensity is given by

$$\frac{I_m}{I_n} = \frac{J_m^2[v \sec \phi (\sin t)/t]}{J_n^2[v \sec \phi (\sin t)/t]} \tag{5}$$

where

$$v = \frac{2\pi\ \mu_1 L}{\lambda}\ , \tag{6}$$

$$t = \frac{\pi L\ \tan\ \phi}{\lambda^*}\ , \tag{7}$$

and ϕ is the inclination of the incident light to the sound waves.

The positions of the diffraction orders when the light is incident at an angle ϕ on the ultrasonic wave are given by

$$\sin(\theta_n + \phi) - \sin\ \phi = \frac{n\lambda}{\mu_0 \lambda^*} \tag{8}$$

where θ_n is the angle of diffraction of the n^{th} order as shown in Figure 1. If the diffraction angle for the first order is

$$\theta_1 = 2\phi \tag{9}$$

conditions for Bragg diffraction are satisfied. Thus, Eq. (8) can be written as

$$\sin\ 2\phi\ \cos\phi + \sin\ \phi\ \cos\ 2\phi - \sin\ \phi = \lambda/\mu_0\lambda^*\ . \tag{10}$$

If ϕ is small enough, then $\cos\ 2\phi \approx 1$. Thus

$$\sin\ 2\phi + \sin\phi - \sin\phi = \frac{\lambda}{\mu_0 \lambda^*} \tag{11}$$

or

$$\lambda = \mu_0 \lambda^*\ \sin\ 2\phi\ . \tag{12}$$

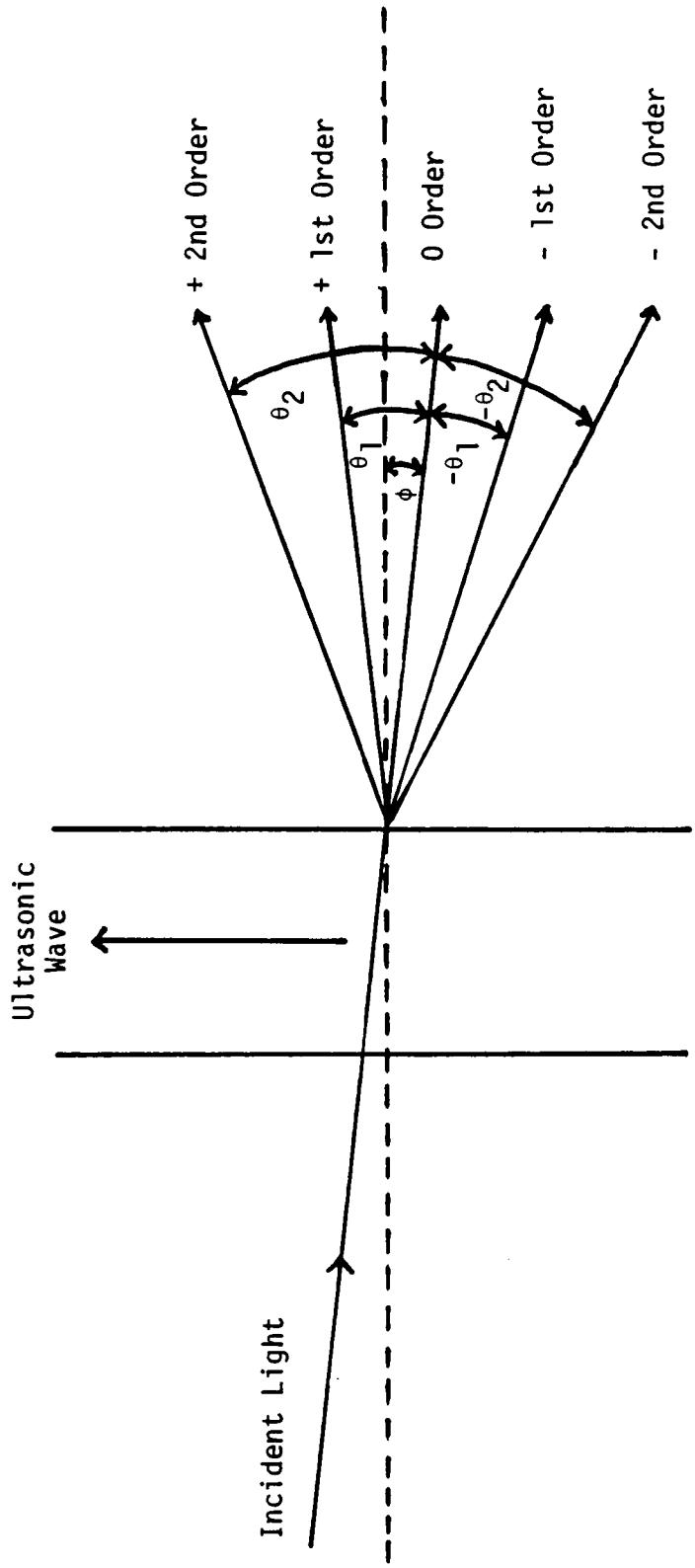


Figure 1. Diffraction orders of light incident on an ultrasonic beam.

This can be written in terms of the Bragg angle ϕ_B as

$$\lambda = 2\mu_0\lambda^* \sin \phi_B \ . \tag{13}$$

This is the ultrasonic Bragg diffraction analogue to the diffraction of x-rays by a crystalline plane, where $\mu_0\lambda^*$ plays the same role as the lattice parameter d. However, additional information exists in this ultrasonic case. The diffraction orders contain information about the ultrasonic wavefront, as will be shown.

II. DIFFRACTION THEORY OF KLEIN, COOK, AND MAYER

The theory of light diffraction by arbitrary periodic ultrasonic waveform, frequency, beam width, and angle of incidence was treated by Klein, Cook, and Mayer (1965). The optical wave equation is solved by resolving the light traveling through the ultrasonic beam into a system of plane waves whose amplitudes are described by a set of difference-differential equations.

They considered plane, monochromatic light waves incident at an angle θ upon a plane ultrasonic beam of width L as shown in Figure 2. Before entering the region containing the sound field, the electric intensity of the light beam can be expressed by

$$E = E_0 \exp[i(\omega t - \mu_0 \vec{k} \cdot \vec{r})] \tag{14}$$

where ω and $\vec{k}$ are the angular frequency and wave vectors of the light in free space, respectively, and μ_0 is the refractive index of the medium. In the region of the sound field, the refractive index varies

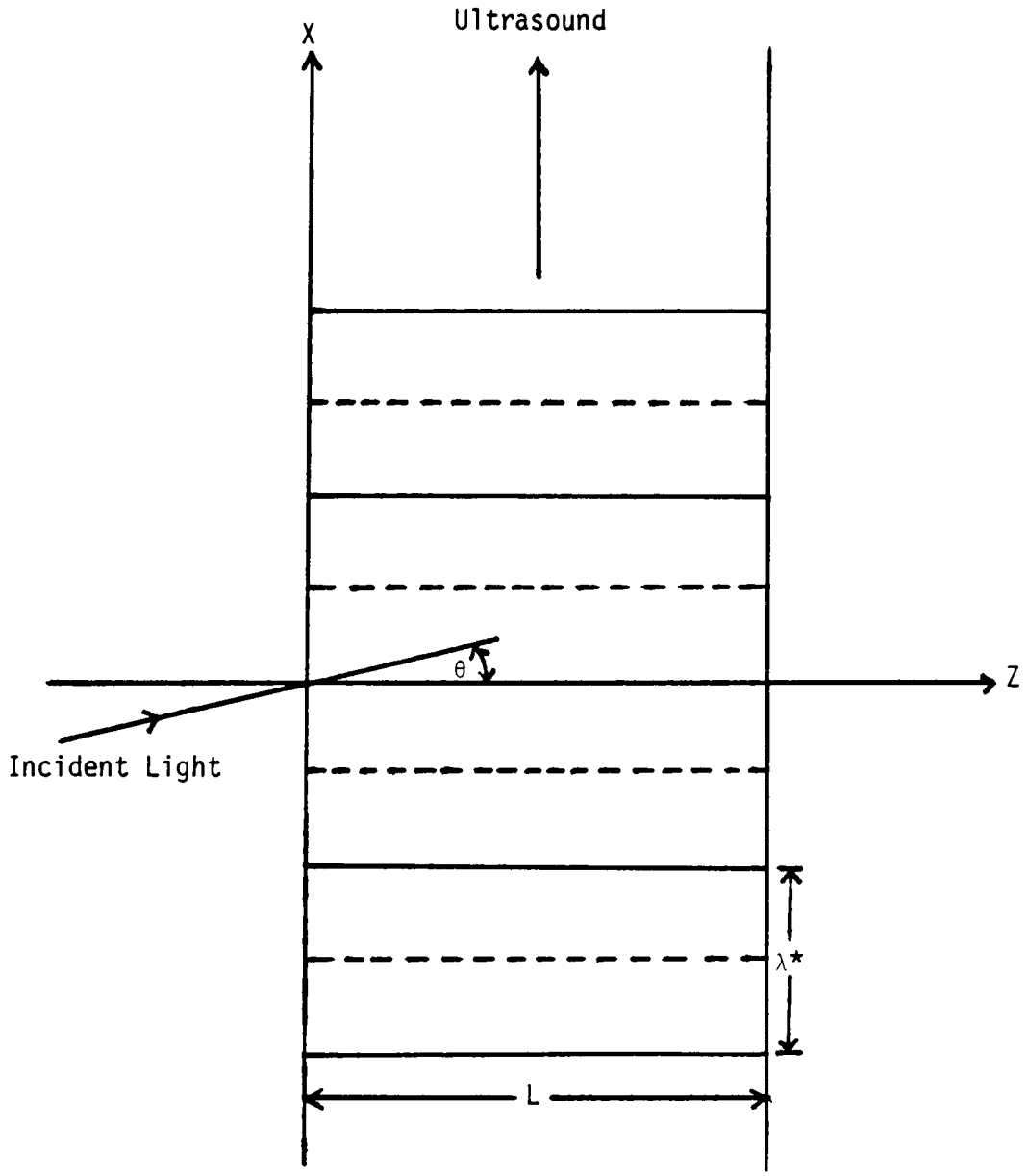


Figure 2. Diagram of the ultrasonic diffraction grating.

in time and space in proportion to the localized changes in the density of the medium. For ultrasonic waves of arbitrary waveform, the refractive index can be written as

$$\mu(x,t) = \mu_0 + \mu' \ . \tag{15}$$

The small change of refractive index produced by the sound wave, μ', is periodic in $(\omega^*t - k^*x)$, where ω^* and k^* are the angular frequency and wave constant, respectively, associated with the fundamental periodicity of the sound waves.

At any point within the liquid in which the ultrasonic beam propagates, the amplitude of the light can be represented by

$$E = A(x,z,t) \exp[i(\omega t - \mu_0 \vec{k} \cdot \vec{r})] \ , \tag{16}$$

where A is a periodic function in the variable k*x. It may thus be expanded in the complex Fourier series

$$A(x,z,t) = \sum_{n=-\infty}^{\infty} \Phi_n(z,t) \exp[-ink^*x] \ , \tag{17}$$

giving

$$E = \sum_{n=-\infty}^{\infty} \Phi_n(z,t) \exp[-ink^*x] \exp[i(\omega t - \mu_0 \vec{k} \cdot \vec{r})] \ , \tag{18}$$

or

$$E = \sum_{n=-\infty}^{\infty} \Phi_n(z,t) \exp[i(\omega t - \vec{k}_n \cdot \vec{r})] \ , \tag{19}$$

where the various propagation vectors of the light are given by

$$\vec{k}_n = \mu_0 \vec{k} + n\vec{k}^* \ . \tag{20}$$

The spatial orientation of these vectors is illustrated in Figure 3.

The propagation of the light through a transparent, nonmagnetic medium is described by the pseudo-homogeneous wave equation

$$\nabla^2 E = \frac{[\mu(x,t)]^2}{c^2} \ \frac{\partial^2 E}{\partial t^2} \ , \tag{21}$$

where the refractive index in the region of the sound field ($0 < z < L$) is written

$$\mu(x,t) = \mu_0 + \sum_{j=1}^{\infty} \mu_j \sin[j(\omega^* t - k^* x) + \delta_j] \ . \tag{22}$$

In Eq. (22), μ_j is the amplitude of the j^{th} Fourier component of the refractive index distribution, and δ_j is its relative phase.

As the electric intensity E is periodic in time and space with the sound field, Eq. (19) can be expanded by letting $\phi_n(z,t) = \phi_n(z) \exp(in\omega^* t)$

$$E = \exp(i\omega t) \sum_{n=-\infty}^{\infty} \phi_n(z) \exp[i(n\omega^* t - \vec{k}_n \cdot \vec{r})] \tag{23}$$

where

$$\vec{k}_n \cdot \vec{r} = \mu_0 k(z \cos\theta + x \sin\theta) + nk^* x \ . \tag{24}$$

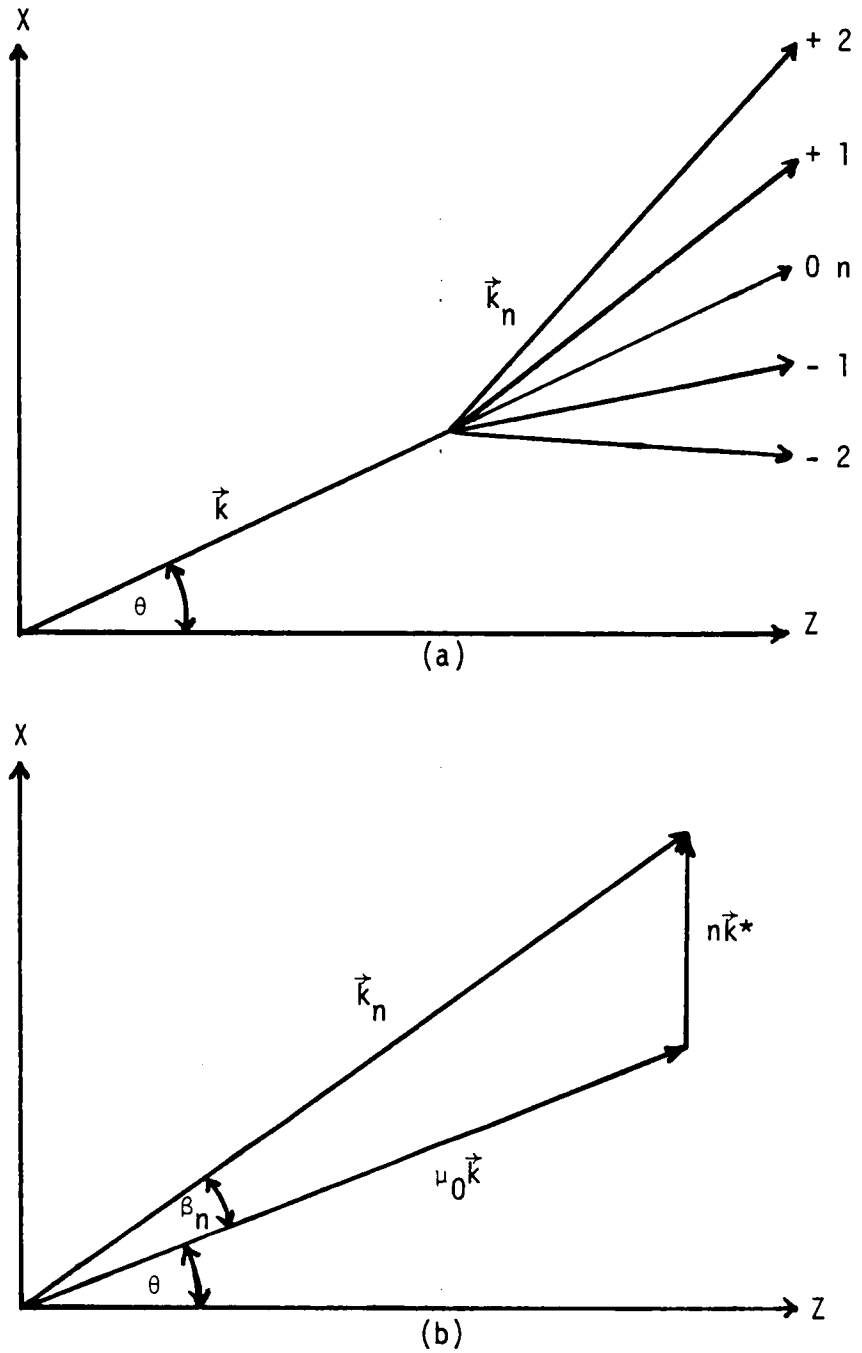


Figure 3. Orientation of the wave vectors in light diffracted by an ultrasonic wave.

Equations (23) and (24) represent an expansion of the diffracted light in plane waves where the index n labels the n^{th} diffraction order. Equation (23) shows that for a progressive wave, the angular frequency of the n^{th} diffraction order is $\omega + n\omega^*$.

By substituting (22), (23), and (24) into (21) and neglecting second-order terms ($\mu' \approx 10^{-5}$), one obtains a set of coupled, difference-differential equations which relate the amplitudes in the plane-wave expansion:

$$\frac{d\phi_n}{dz} + \frac{1}{2L} \sum_{j=1}^{\infty} v_j [\phi_{n-j} \exp(i\delta_j) - \phi_{n+j} \exp(-i\delta_j)]$$

$$= i \frac{nQ}{2L} (n-2\alpha)\phi_n \qquad (25)$$

where

$$v_j = k \mu_j L , \qquad (26)$$

$$Q = \frac{k^{*2} L}{\mu_0 k} \approx \frac{k^{*2} L}{\mu_0 k \cos \theta} , \qquad (27)$$

$$\alpha = - \left(\frac{\mu_0 k}{k^*}\right) \sin \theta . \qquad (28)$$

Equation (25) is to be solved subject to the boundary conditions at Z = 0:

$$\phi_0 = 1 , \qquad (29)$$

$$\phi_n = 0 \quad (n \neq 0) . \qquad (30)$$

For a sinusoidal sound field (25) becomes

$$\frac{d\phi_n}{dZ} + \frac{v}{2L}[\phi_{n-1} - \phi_{n+1}] = \frac{inQ}{2L}(n - 2\alpha)\phi_n \ . \tag{31}$$

This expression and its solution are best described by first considering the significance of the various parameters.

Significance of Parameters

The variable v. The acoustical pressure amplitude determines the light intensity distribution in the diffraction pattern. An analysis of the light intensity distribution in the diffraction orders, then, allows one to calculate the pressure amplitude.

The variation in refractive index produced by the sound field, μ_1, can be related to the acoustical pressure amplitude p by

$$\mu_1 = \left(\frac{\partial \mu}{\partial p}\right)_S p \tag{32}$$

where $\left(\frac{\partial \mu}{\partial p}\right)_S$ is the adiabatic piezooptic coefficient. The values of $\left(\frac{\partial \nu}{\partial p}\right)_S$ have been measured for a limited number of liquids (Raman and Venkateraman, 1939).

From (26) and (32), v is related to the acoustical pressure by

$$v = k\left(\frac{\partial \mu}{\partial p}\right)_S pL \ . \tag{33}$$

The range of values of the parameter v in the usual experimental situation is from zero to ten, although it is easy to obtain higher values at lower ultrasonic frequencies.

The variable α. The variable α is a measure of the angle of incident light on the sound field. The negative sign in Eq. (28) is chosen so that Bragg diffraction into the positive first order occurs for $\alpha = +\frac{1}{2}$, and into the negative order when $\alpha = -\frac{1}{2}$. The labeling of the orders is such that the positive orders are those in the direction of sound propagation.

The parameter Q. The parameter Q characterizes the transition from Raman-Nath diffraction conditions to Bragg diffraction conditions. The quantities on which Q depend (k, k*, μ_0, and L) are normally constant in a given experimental situation. The general nature of the diffraction process in the Raman-Nath region can be described by this parameter because for very large Q (high frequencies) diffraction is not found to occur at normal incidence.

The parameter Q is a measure of the differences in phase of the various partial waves due to their different directions of propagation. When the phase difference in these waves becomes large (say $Q > 1$), the diffracted light tends to remain in the lower orders. Since the amount of energy transfer between the waves depends on the coupling constants and the degree of synchronization of the waves, the parameter Q can be used to express the degree of synchronization of the various waves. For larger values of Q there is less synchronization. If the waves are nearly synchronous, i.e., the phase difference between the waves is nearly constant, energy transfer between the various orders readily occurs. This condition is found in the Raman-Nath region. If the waves are highly nonsynchronous the energy transfer is extremely small

for all orders except that going from the zero order to the first order. This phenomenon can be explained by using Eq. (31). By substituting Eq. (28) into Eq. (31), the right-hand side of Eq. (31) becomes

$$i[nk^*\tan\theta + n^2Q/2L]\phi_n \ .$$

Since Q is large when the waves are highly nonsynchronous, the diffraction effects are found to be asymmetric for oblique incidence. This term vanishes for $(in\ k^*\tan\theta + in^2Q/2L) = 0$. It vanishes uniquely for the zero order which initially contains all of the light. It also vanishes when $\tan\theta = -nQ/2k^*L$. By substituting the expression for Q, Eq. (27), one recognizes $\tan\theta = -nQ/2k^*L$ is equal to the Bragg diffraction equation $n\lambda = 2\mu_0\lambda^*\sin\theta$. This means that synchronism occurs for those directions θ satisfying the Bragg conditions. More detailed examination reveals that synchronism is most complete for $n = 1$, the first Bragg diffraction order. For $n = -1$ and $n = 2$, the waves are partially synchronous, and one also finds a small amount of light diffracted in these orders.

For the region $Q < 0.5$, analytic solutions of Eq. (31) which are equivalent to the results of Raman and Nath was found [Klein et al. (1965)].

In the region, $0.5 < Q < 10$, which is the experimental situation required for Bragg diffraction, an analytic solution of Eq. (31) has not been obtained. The N^{th} order approximation method of Leroy and Blomme is used in this dissertation to get expressions for the

amplitudes and intensities of order 0, ±1, and -2 at Bragg incidence and in the vicinity of the Bragg angle [Blomme and Leroy (1986)].

Solutions of the Difference-Differential Equations for Raman and Nath Region ($Q << 1$)

As the number of diffraction orders is usually small (10 or less), the maximum absolute value of n is also usually small. For moderate angles of incidence at low frequencies, the numerical value of α can be very large. This permits one to neglect the first term of the right-hand side of Eq. (31), while the second term which contains the angular dependence must be retained.

Equation (31) thus becomes

$$\frac{d\phi_n}{dZ} + \frac{v}{2L}[\phi_{n-1} + \phi_{n+1}] = -i\,\frac{nQ}{L}\,\alpha\,\phi_n \,. \tag{34}$$

Using the identity for ordinary Bessel functions,

$$J_n(x) = \frac{x}{2n}(J_{n-1} + J_{n+1}) \,, \tag{35}$$

it can be shown that the solution of (34) is

$$\phi_n = \exp[-i\,\frac{nQ\alpha Z}{2L}]J_n[\frac{2v}{Q\alpha}\sin(\frac{Q\alpha Z}{2L})] \,, \tag{36}$$

or at $Z = L$, the intensity of n^{th} diffraction orders is

$$I_n = |\phi_n|^2$$

$$= J_n^{\,2}[v\,\frac{\sin(Q\alpha/2)}{Q\alpha/2}] \,. \tag{37}$$

At normal incidence $\alpha = 0$ Eq. (37) reduces to

$$I_n = J_n^2(v) \ . \tag{38}$$

This result is identical with that of Raman and Nath.

The ultrasonic fields described by the condition Q << 1 are equivalent to optical gratings which produce only a modulation of the phase of light passing through them. Exploring the light distribution at the exit plane (Z = L), one finds

$$\begin{aligned} I(x,L,t) &= |E(x,L,t)|^2 \\ &= \Big| \sum_{n=-\infty}^{\infty} J_{-n}(v) \exp[in(\omega^* t - k^* x)] \Big|^2 \\ &= 1 \ , \end{aligned} \tag{39}$$

which means that there is no amplitude modulation at this plane. However, the light is modulated in phase as can be seen by investigating the phase of light in a version of (23)

$$\begin{aligned} E = \sum_{n=-\infty}^{\infty} & J_{-n}(v) \exp[in(\omega^* t - k^* x)] \\ & \cdot \exp[i(\omega t - \mu_0 kL)] \ . \end{aligned} \tag{40}$$

Ignoring the constant phase factor in the last exponential, and exploring the dependence of the phase angle Ω of E on the variable $(\omega^* t - k^* x)$, one finds

$$\tan \Omega = \frac{\sum_{n=-\infty}^{\infty} J_{-n}(v) \sin n(\omega^* t - k^* x)}{\sum_{n=-\infty}^{\infty} J_{-n}(v) \cos n(\omega^* t - k^* x)} \ , \tag{41}$$

or

$$\tan \Omega = \frac{-\sin[v \sin(\omega*t - k*x)}{\cos[v \sin(\omega*t - k*x)]} , \tag{42}$$

and the phase of E is

$$\Omega = -v \sin(\omega*t - k*x) . \tag{43}$$

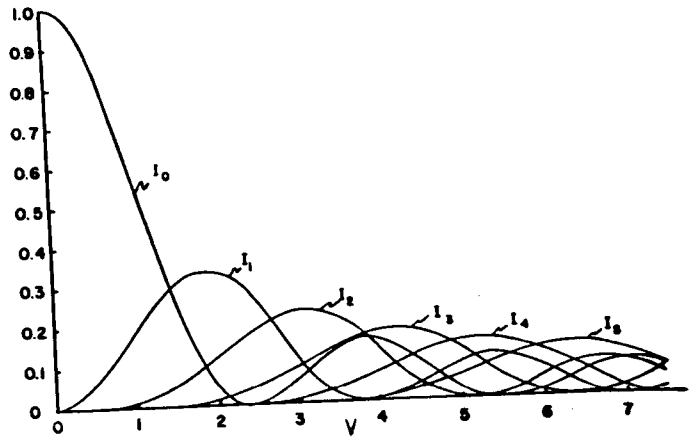
This agrees with the early observation of Raman and Nath that a sound beam of narrow width and low frequencies could be considered as an optical phase grating. The parameter v, known as the Raman and Nath parameter, describes completely the diffraction in this case. It measures the degree of phase modulation of the light produced by the sound beam.

The intensities of the first few diffraction orders as a function of v for $\alpha = 0$ (normal incidence) are shown in Figure 4(a) [Klein, Cook, and Mayer (1965)].

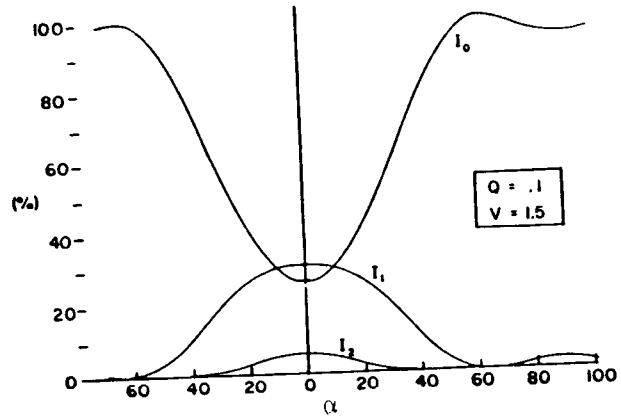
Since the value $[\sin(Q\alpha/2)/(Q\alpha/2)]$ in Eq. (37) is a symmetric function in α, the intensity of a particular order as a function of angle of incidence is symmetric about normal incidence ($\alpha = 0$). This is shown in Figure 4(b) [Klein, Cook, and Mayer (1967)].

III. DIFFRACTION THEORY OF BLOMME AND LEROY FOR THE BRAGG REGION

Blomme and Leroy defined new parameters which are slightly different from those of Klein, Cook, and Mayer. The new parameters



(a) Function of Raman-Nath Parameter v



(b) Function of Incident Angle α

Figure 4. Light intensities of diffraction orders under Raman-Nath conditions.

which are especially useful in the approximation method of Blomme and Leroy are defined by

$$\rho = \frac{\lambda^2 \cos^2\theta}{\mu_0 \mu_1 \lambda^{*2}} \approx \frac{\lambda^2}{\mu_0 \mu_1 \lambda^{*2}} \tag{44}$$

and

$$b = \frac{2\lambda \sin\theta}{\mu_1 \lambda^*} . \tag{45}$$

With these parameters and $v = k \mu_1 L$, Eq. (31) becomes

$$2 \frac{d\phi_n}{dv} + (\phi_{n+1} - \phi_{n-1}) = in(n\rho - b)\phi_n . \tag{46}$$

In order to solve (46) Blomme and Leroy applied the NOA-method (N^{th} Order Approximation) by assuming that the ultrasonic power is not strong enough to excite diffraction orders different from 0, ±1, and -2 for incidence angles in the neighborhood of the first Bragg angle ($0 < \theta < 2\beta$ and $\beta = \frac{\lambda}{2\mu_0 \lambda^*}$).

Under these conditions the amplitudes ϕ_{-2}, $\phi_{\pm 3}$, ... vanish and (46) reduces to the simple set of difference-differential equations

$$2D\ \phi_{-1} + \phi_0 = i(\rho + b)\phi_{-1} , \tag{47}$$

$$2D\ \phi_0 - \phi_{-1} + \phi_1 = 0 , \tag{48}$$

$$2D\ \phi_1 - \phi_0 + \phi_2 = i(\rho - b)\phi_1 , \tag{49}$$

and

$$2D\ \phi_2 - \phi_1 = 2i(2\rho - b)\phi_2 \ , \tag{50}$$

where D represents derivation with respect to v. Equations (47) through (50) can be solved for the amplitudes of the diffraction orders.

$$\phi_1 = 2D\ \phi_2 - 2i(2\rho - b)\phi_2 \ , \tag{51}$$

$$\phi_0 = 2D\ \phi_1 + \phi_2 - i(\rho - b)\phi_1 \ , \tag{52}$$

$$\phi_{-1} = 2D\ \phi_0 + \phi_1 \ , \tag{53}$$

and

$$\begin{aligned} &16D^4\ \phi_2 - 16i(3\rho - b)D^3\ \phi_2 + 4(3 + b^2 + 4\rho b - 9\rho^2)D^2\ \phi_2 \\ &\quad + 2i(4\rho^3 - 2\rho^2 b - 4\rho b^2 + 2b^3 - 11\rho + 3b)D\ \phi_2 \\ &\quad - (8\rho^2 - 4\rho b - 1)\phi_2 = 0 \ . \end{aligned} \tag{54}$$

The last equation determines ϕ_2. The solution of (54) can be written as

$$\phi_2 = \sum_{j=1}^{4} C_j \exp(i\ r_j\ v) \tag{55}$$

where $C_1, \ldots, C_4$ are arbitrary constants which still remain to be determined and $r_1, \ldots, r_4$ are the real roots of the characteristic equation

$$r^4 + a_1 r^3 + a_2 r^2 + a_3 r + a_4 = 0 \ , \tag{56}$$

in which

$$a_1 = b - 3\rho \ , \tag{57}$$

$$a_2 = \frac{1}{4}\,(9\rho^2 - b^2 - 4\rho b - 3) \ , \tag{58}$$

$$a_3 = \frac{1}{8}\,(2\rho^2 b + 4\rho b^2 - 4\rho^3 - 2b^3 + 11\rho - 3b) \ , \tag{59}$$

$$a_4 = \frac{1}{4}\,\rho(b - 2\rho) + \frac{1}{16} \ . \tag{60}$$

The expressions for the other amplitudes ϕ_1, ϕ_0, and ϕ_{-1} from (51) through (53) and are given by

$$\phi_1 = 2i \sum_{j=1}^{4} c_j A_j \exp(ir_j v) \ , \tag{61}$$

$$\phi_0 = - \sum_{j=1}^{4} c_j B_j \exp(ir_j v) \ , \tag{62}$$

and

$$\phi_{-1} = -2i \sum_{j=1}^{4} c_j C_j \exp(ir_j v) \tag{63}$$

where

$$A_j = r_j - 2\rho + b \ , \tag{64}$$

$$B_j = 4r_j^2 - 2(5\rho - 3b)r_j + 4\rho^2 - 6\rho b + 2b^2 - 1 \ , \tag{65}$$

and

$$C_j = r_j(B_j - 1) + 2\rho - b \ . \tag{66}$$

Taking into account the boundary conditions $\phi_n(0) = \delta_{no}$, a set of equations is obtained for determining the constants c_j:

$$\phi_2(0) = \sum_{j=1}^{4} c_j = 0 \ , \tag{67}$$

$$\phi_1(0) = \sum_{j=1}^{4} c_j A_j = 0 \ , \tag{68}$$

$$\phi_0(0) = \sum_{j=1}^{4} c_j B_j = 1 \ , \tag{69}$$

and

$$\phi_{-1}(0) = \sum_{j=1}^{4} c_j C_j = 0 \ . \tag{70}$$

The solution of this system which can be found by applying Cramer's rule for linear systems of algebraic equations and the relation $\sum r_j = -a_1$ is given by

$$c_j = \frac{b - \rho - r_j}{4(r_i - r_j)(r_k - r_j)(r_\ell - r_j)} \tag{71}$$

where i, j, k, and ℓ take on different values from each other from the set {1, 2, 3, 4}. Finally, the intensities of the diffracted orders follow from $I_n = \phi_{-n}\phi_{-n}^*$:

$$I_{-2} = \sum c_j^2 + 2 \sum_{i<j}^{4} c_i c_j \cos[(r_i - r_j)v] \ , \tag{72}$$

$$I_{-1} = 4 \sum c_j^2 A_j^2 + 8 \sum_{i<j}^{4} c_i c_j A_i A_j \cos[(r_i - r_j)v] \ , \tag{73}$$

$$I_0 = \sum c_j^2 B_j^2 + 2 \sum_{i<j}^{4} c_i c_j B_i B_j \cos[(r_i - r_j)v] , \qquad (74)$$

and

$$I_1 = 4 \sum c_j^2 C_j^2 + 8 \sum_{i<j}^{4} c_i c_j C_i C_j \cos[(r_i - r_j)v] . \qquad (75)$$

The sum of Eqs. (72) through (75) is equal to unity which is the total input of light intensity.

Numerical solutions of Eqs. (72) through (75) are used in Chapters III and IV to explain Bragg diffraction. In addition, they are used to explain both first-order and second-order Bragg imaging which can be observed when Bragg diffraction takes place.

CHAPTER III

EXPERIMENTAL INVESTIGATION OF BRAGG IMAGING

I. APPARATUS

Raman-Nath Diffraction System

A block diagram of the experimental arrangement for measuring Raman-Nath diffraction is shown in Figure 5. An RF signal is generated by a VFO controlled oscillator having a maximum output of approximately 100 watts. The high voltage, and hence the output power, is controlled by an external Variac. X-cut quartz transducers were used and driven at their fundamental frequency as well as their odd harmonics.

A square quartz transducer is placed in a tank filled with water. An absorber is located at the end of the tank to reduce the amplitude of the reflected ultrasonic wave. A helium-neon laser is used as a light source. The wavelength of the light is 6328 Å. The beam passes through the sound field as shown in Figure 5. Since the width of the laser beam is very small and collimated, a diffraction pattern is obtained without the addition of a slit and collimator. A diffraction pattern is formed in the plane of the photomultiplier which is used to measure the intensity of the diffraction orders.

Bragg Diffraction Conditions

The Bragg diffraction conditions (Eq. (2)) can be demonstrated by measuring the distance, D, from the point of emergence, p, of the

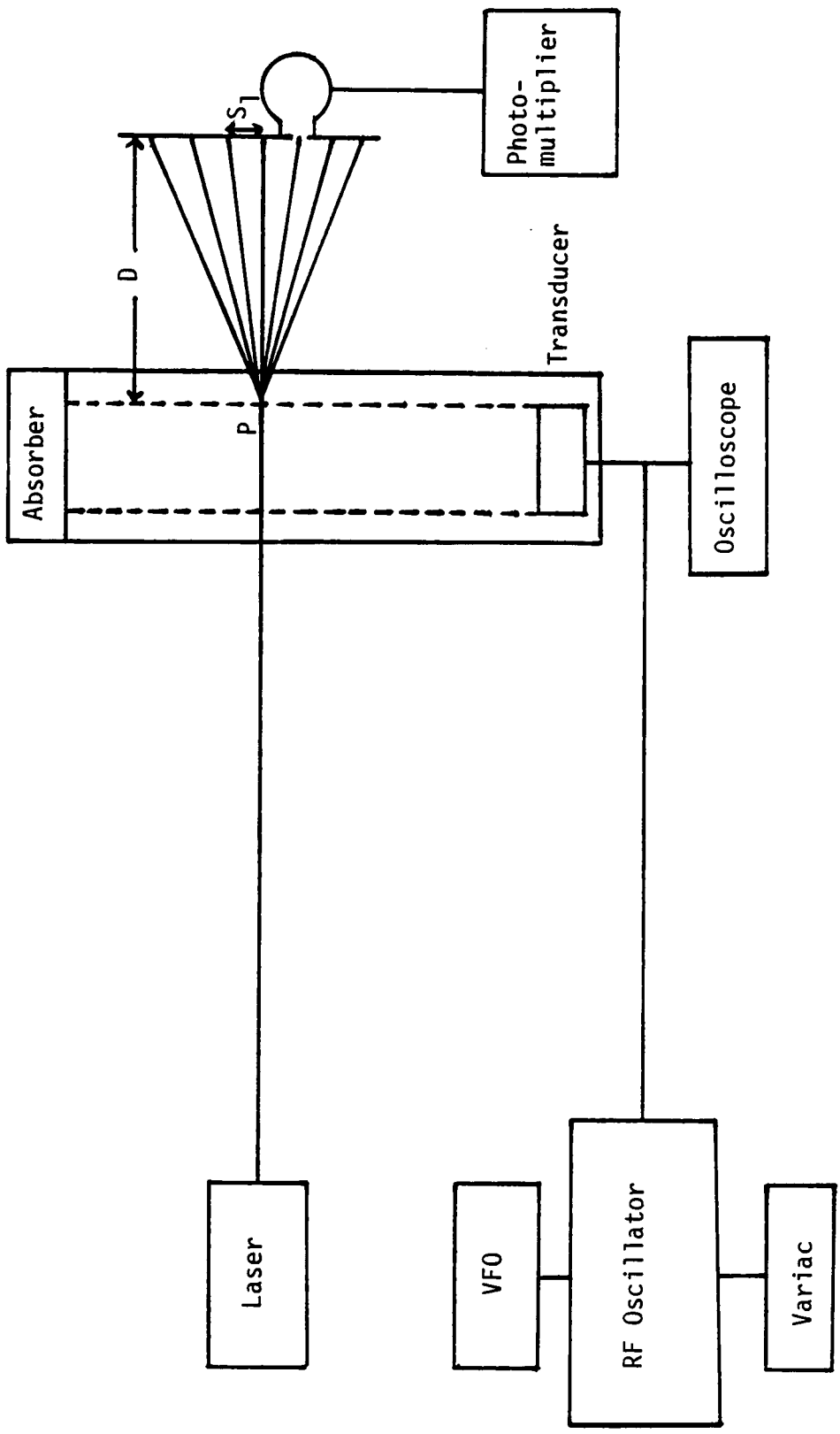


Figure 5. Experimental arrangement for Raman-Nath diffraction of light by ultrasonic waves.

light from the ultrasonic beam (Figure 5) to the screen and the distance, S_1, from the zero diffraction order to the first order. In the experiment D is 10 m and frequencies of ultrasound are 2, 4, 6, 10, 12, 15, 20, and 28 MHz. Table I shows theoretical and experimental Bragg angles. From this table it is obvious that Eq. (1) must be changed to Eq. (2), since the theoretical values in Column 2 were calculated from Eq. (2). In other words, the refractive index μ_0 must be considered because the wavelength of light must be measured in the liquid medium (water), as suggested by Klein, Cook, and Mayer (1965).

Intensities of Diffraction Orders

In order to measure intensities of diffraction orders under Raman-Nath conditions, a photomultiplier is used at a distance of 50 cm from the water tank. The Raman-Nath parameter v is increased by increasing the output voltage of the transducer. Two different 2 MHz transducers, 2.4 cm and 4.8 cm in width, are used.

Intensities of diffraction orders for different values of v are shown in Figure 6. In this figure, dots, triangles, and crosses represent experimental values of the zero, first, and second diffraction orders, respectively. Q values of the 2.4 cm and 4.8 cm transducers are 0.1 and 0.3, respectively, at 2 MHz.

By comparing (a) and (b) in Figure 6, one can see that the lower Q value gives better agreement with Raman-Nath diffraction theory in the Raman-Nath region. For frequencies above 12 MHz Q approaches larger values and the diffraction is no longer in the Raman-Nath region in which the intensity of light is proportional to the square of a Bessel function, but is in the Bragg region. From these

Table I. Comparison of Theoretical and Experimental Bragg Angles

Frequency (MHz)	Theoretical Bragg Angle (°)	Experimental Bragg Angle (°)	S_1 (cm)
2	1.8×10^{-2}	1.7×10^{-2}	0.3
4	3.6×10^{-2}	3.4×10^{-2}	0.6
6	5.5×10^{-2}	5.7×10^{-2}	1.0
10	9.1×10^{-2}	9.2×10^{-2}	1.6
12	1.1×10^{-1}	1.2×10^{-1}	2.0
15	1.4×10^{-1}	1.4×10^{-1}	2.5
20	1.8×10^{-1}	1.8×10^{-1}	3.2
28	2.5×10^{-1}	2.6×10^{-1}	4.6

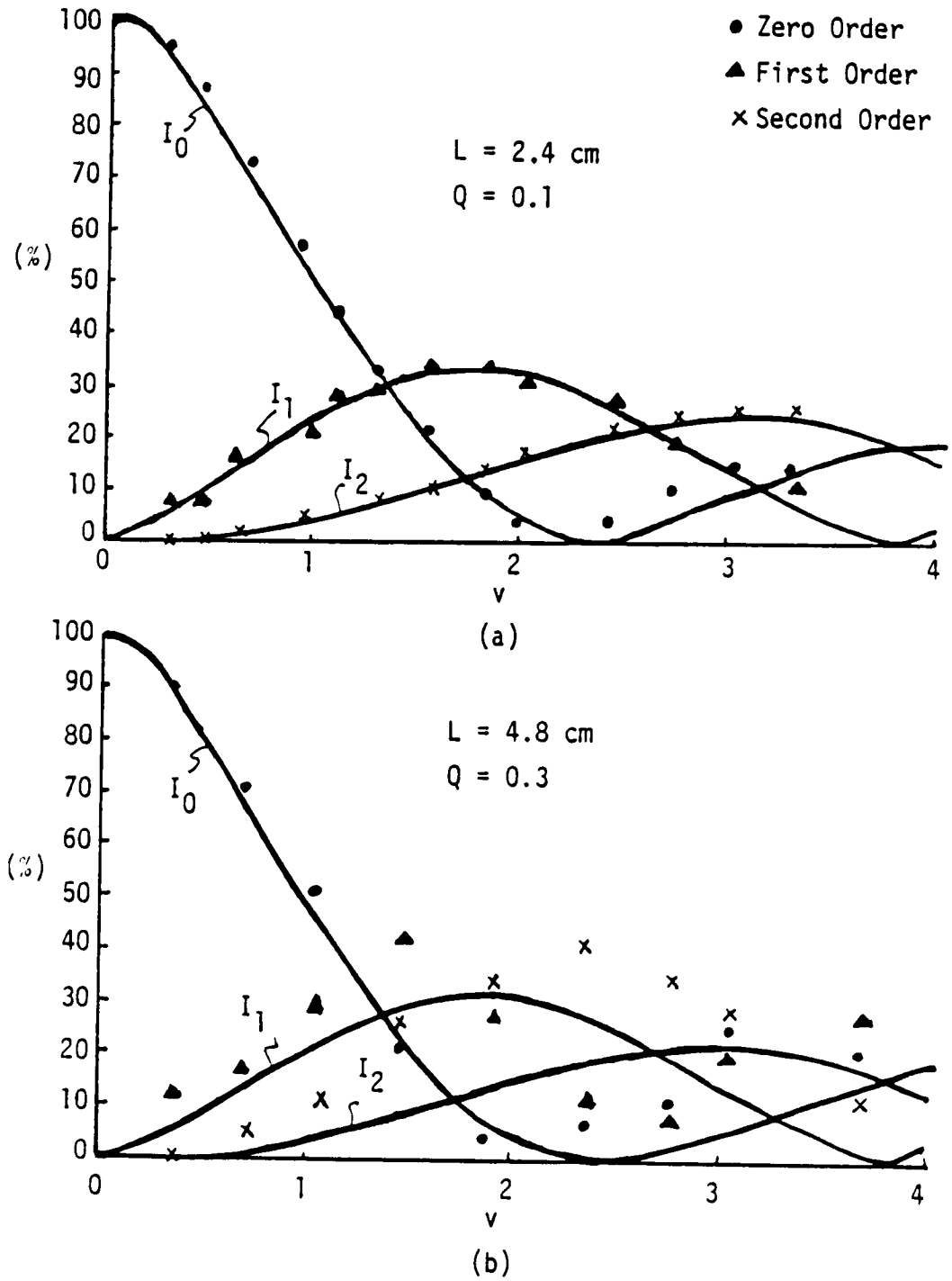


Figure 6. Intensities of diffraction orders plotted as a function of Raman-Nath parameter v.

results one can see that the parameter Q defined by Klein, Cook, and Mayer is a nice parameter to define the transition from Raman-Nath conditions to Bragg conditions in diffraction phenomena.

Bragg Diffraction System

In the Bragg diffraction region the objective of the experiments is to understand the origin of certain Bragg images. To do this, it is adequate to observe qualitative agreement between theoretical predictions of light intensities and intensity distributions observed in the images. For this reason the photomultiplier is not used in the Bragg region. For the purpose of this thesis, photographic recording of the images is adequate.

A block diagram of the experimental arrangement is given in Figure 7. The electronics and ultrasonic source are the same as described in the Raman-Nath Diffraction System; however, several optical lenses are required. The beam is collimated by a laser beam expander (1). A cylindrical lens (2) is located to make a wedge of light converge to a vertical line just beyond the tank. In this way, the positive and negative Bragg diffraction orders are observed simultaneously because light is incident at both $+\phi_B$ and $-\phi_B$. Lenses (3) and (4) are also cylindrical lenses which are used to adjust the width of the diffraction orders on the viewing screen. Photographs of the diffraction pattern can be made simply by putting a camera back with a focal plane shutter in place of the viewing screen. A photograph of this arrangement is shown in Figure 8 in which both camera and photomultiplier are visible.

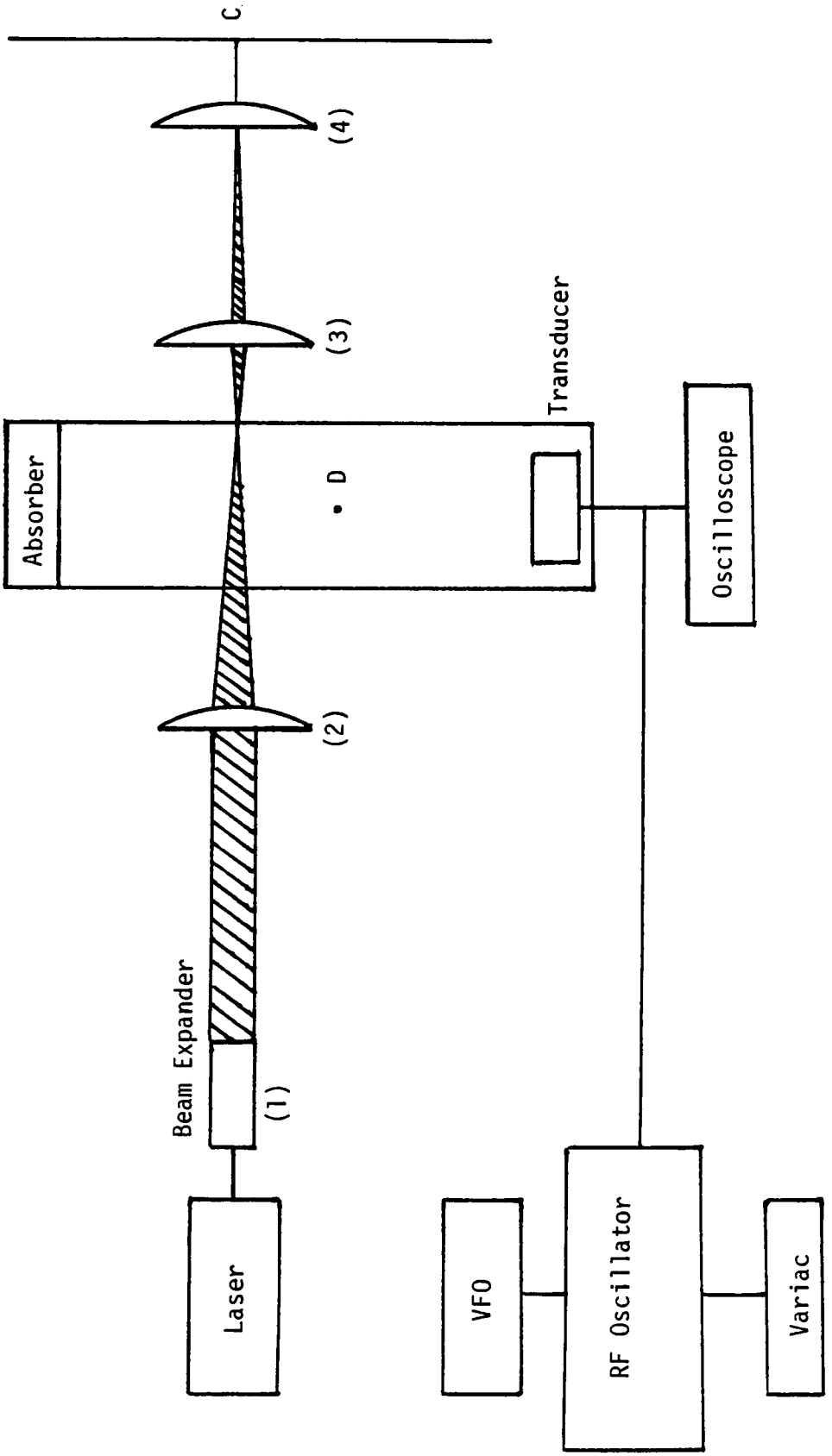


Figure 7. Experimental arrangement of the Bragg diffraction system.

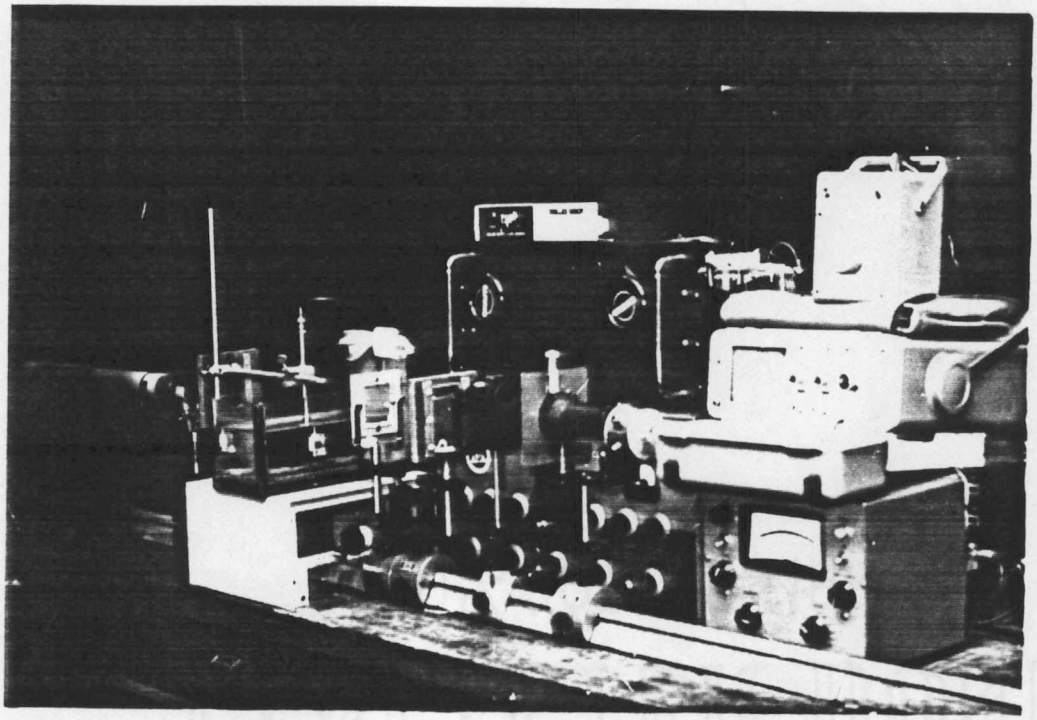


Figure 8. Photograph of experimental arrangement of Bragg diffraction system.

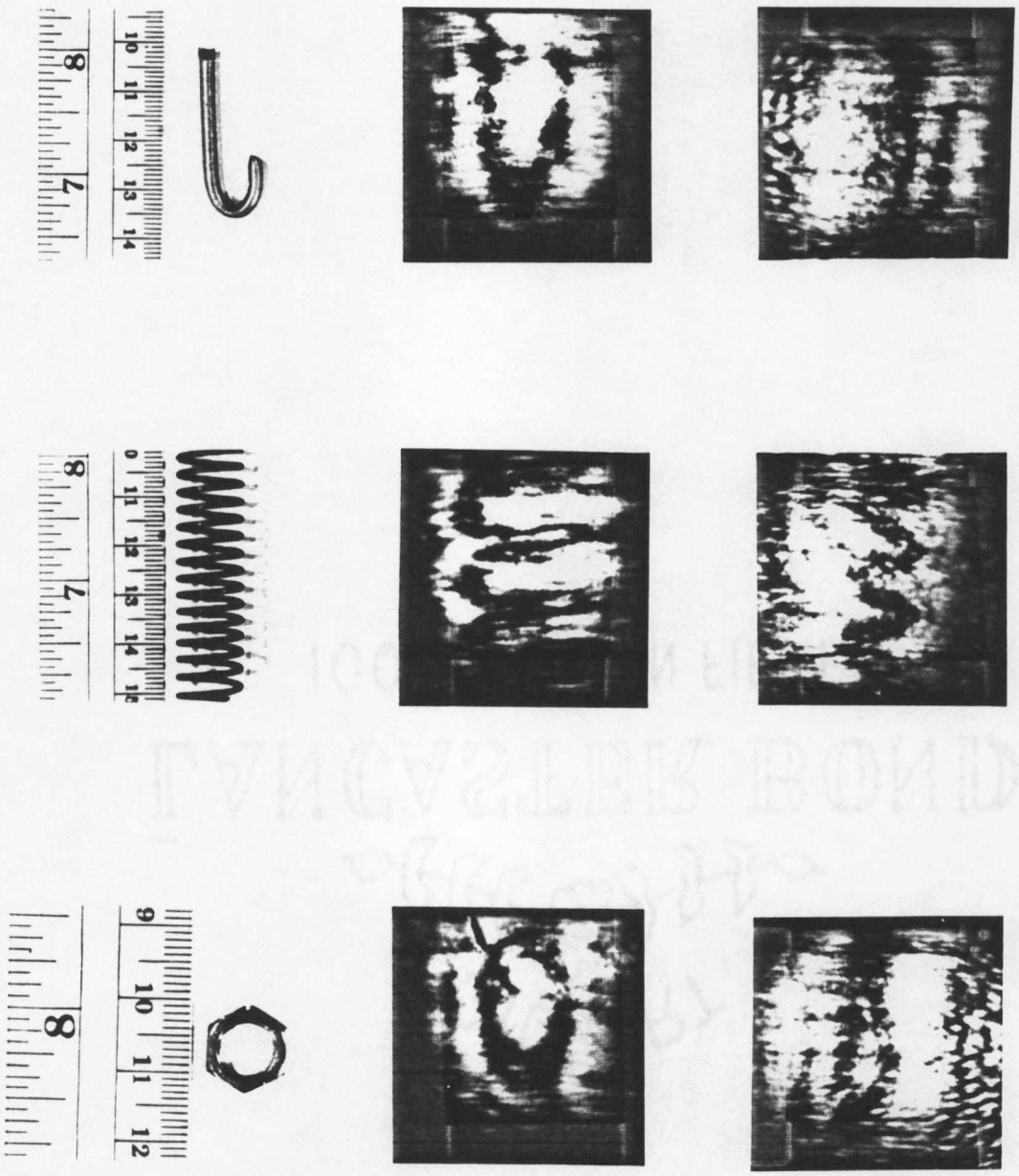
Bragg imaging is obtained by placing an object to be imaged in the ultrasonic field between the transducer and the light beam at point D in Figure 7 and observing the imaging in the diffraction orders on the viewing screen.

II. EXPERIMENTAL OBSERVATIONS

First-Order Bragg Imaging

The experimental arrangement shown in Figure 8 is used to observe first-order Bragg diffraction. Objects are placed in the ultrasonic field between transducer and light beam. Images of the objects are found within the first diffraction orders. Photographs of the objects used in these investigations are shown in Figure 9(a) and Figure 9(b) and are photographs of the first diffraction orders. A frequency of 20 MHz and transducer width of L = 2.4 cm is used to obtain these photographs. The images in Figure 9(c) are photographs of the first diffraction orders taken with 10 MHz and transducer width of L = 4.8 cm. The imaging in Figure 9(c) is less distinct than in Figure 9(b). This results from the fact that with 20 MHz (Q = 12.8) the diffraction is in the Bragg region; with 10 MHz (Q = 6.4) the diffraction is intermediate between the Bragg and Raman-Nath regions where conditions are not favorable for imaging.

With imaging observed at the frequencies 2, 4, 6, 10, 12, 18, 20, and 28 MHz, the quality of the images in the first diffraction orders improves with increasing frequency, with the best images occurring for 18 MHz and above. For frequencies of 2 and 4 MHz, images are faint. They are easily masked out by increasing the ultrasound



(a) (b) (c)

Figure 9. Photographs of objects and their first-order Bragg images: (a) hook, spring, and nut; (b) frequency 20 MHz and width of ultrasound 2.4 cm; (c) frequency 10 MHz and width of ultrasound 4.8 cm.

intensity, which increases the intensity of the "regular" diffraction orders. Above 6 MHz the images are of a quality approaching those in Figure 9(c). At 28 MHz zero, minus first, and plus first orders are observed. First order images of a hook, a spring, and a nut taken at 28 MHz are shown in Figure 10. From this figure one can see that the quality of first-order Bragg images clearly becomes better with higher frequency of ultrasound.

The images in the positive orders are always mirror images of those in the corresponding negative orders. Photographs in Figure 11 are taken to show both the positive and negative first orders. Images of the hook in these orders are seen to be mirror images.

Second-Order Bragg Imaging

For frequencies below 18 MHz, it is noted that as the transducer voltage is increased, higher diffraction orders become visible. These orders, in general, contain light which has been diffracted both as "Raman-Nath" and as "Bragg" diffraction. As the frequency is decreased, these orders are observable for lower transducer voltages, but the imaging may be less distinct. Multiple images are observed in the higher diffraction orders. There are two images in the second order as in Figure 12. The appearance of these images was noted by Franklin D. Martin (1971) and an explanation of their origin was attempted. The explanation given in this thesis differs from that of Martin. It is based on the theory of Blomme and Leroy and is capable of more detailed treatment of the subject than Martin's explanation was capable of.

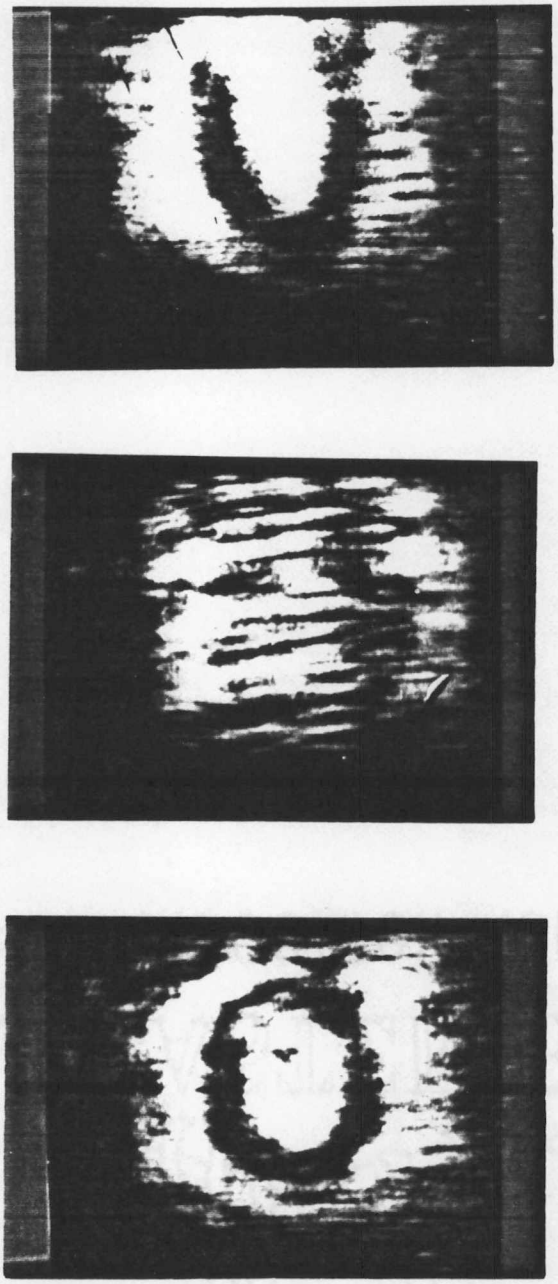


Figure 10. Photographs of first-order Bragg images of hook, spring, and nut, frequency 28 MHz.

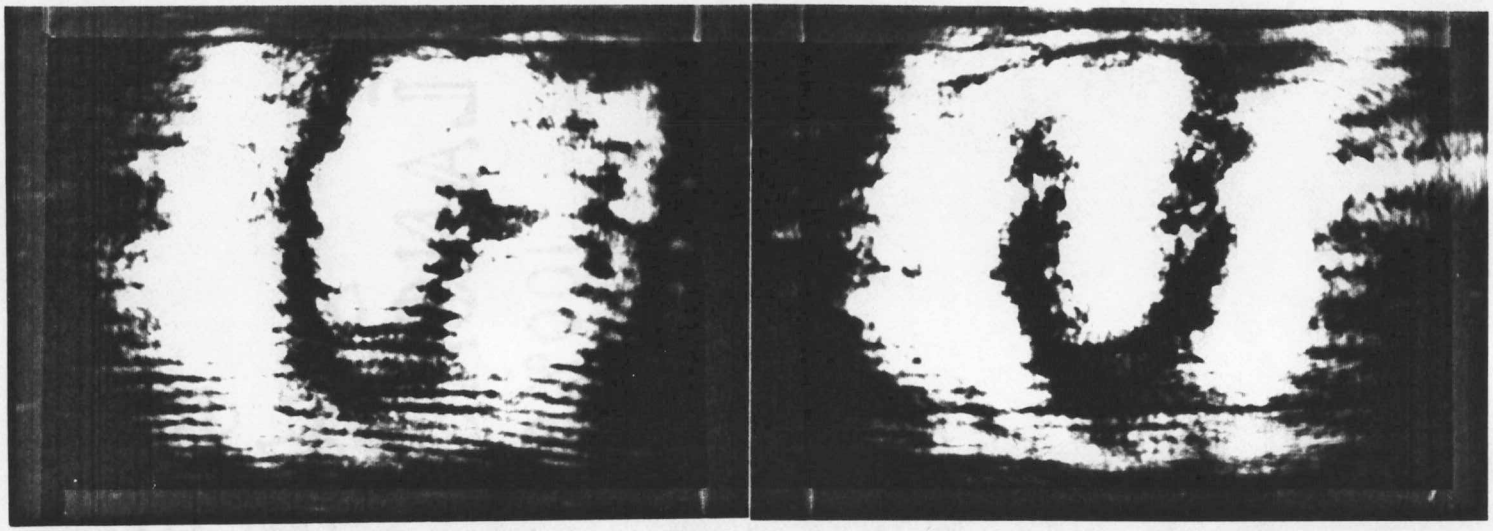


Figure 11. Photographs of positive and negative first-order Bragg images of a hook, frequency 20 MHz.

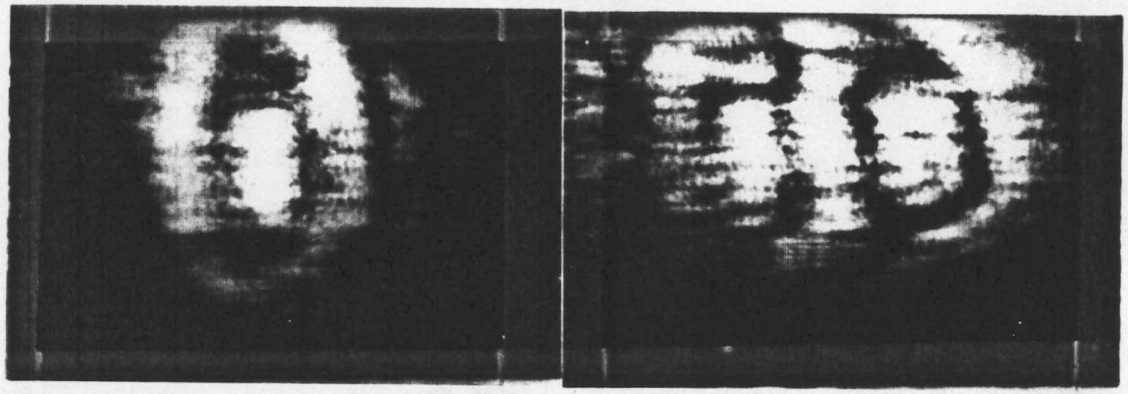


Figure 12. Photographs of first- and second-order images of a nut, frequency 12 MHz.

CHAPTER IV

ANALYSIS OF BRAGG IMAGING

The existence of Bragg images in the first order and second order has been demonstrated in Chapter III. In this chapter Blomme and Leroy's theoretical equations are used to interpret the quality of Bragg imaging in the first order and the existence of two Bragg images in the second order. Before starting the interpretation, however, it is necessary to point out the relationship between theoretically defined diffraction orders and those defined experimentally. In making the theoretical definitions one can assume the light to be incident at the Bragg angle with either a positive or a negative incident angle. In the experiment the light is incident at both angles simultaneously. The experimental diffraction orders, then, can contain light from more than one theoretically defined order. For example, in Figure 13 the incident light labelled E_1 is incident at an angle β. The zero order of the E_1 component emerges at an angle β. Likewise, the incident light labelled E_2 is incident at an angle $-\beta$, and the zero order of this component emerges at an angle $-\beta$. This is the direction of the -1 order of the E_1 light, however. In Figure 13 the light intensity in the orders is labelled with two subscripts: the first identifying the origin (E_1, E_2, E_3, or E_4) and the second labelling the order number consistent with the theory of Blomme and Leroy (1984). As can be seen, illuminating the entire range of angles gives rise to the possibility of intensity maxima of

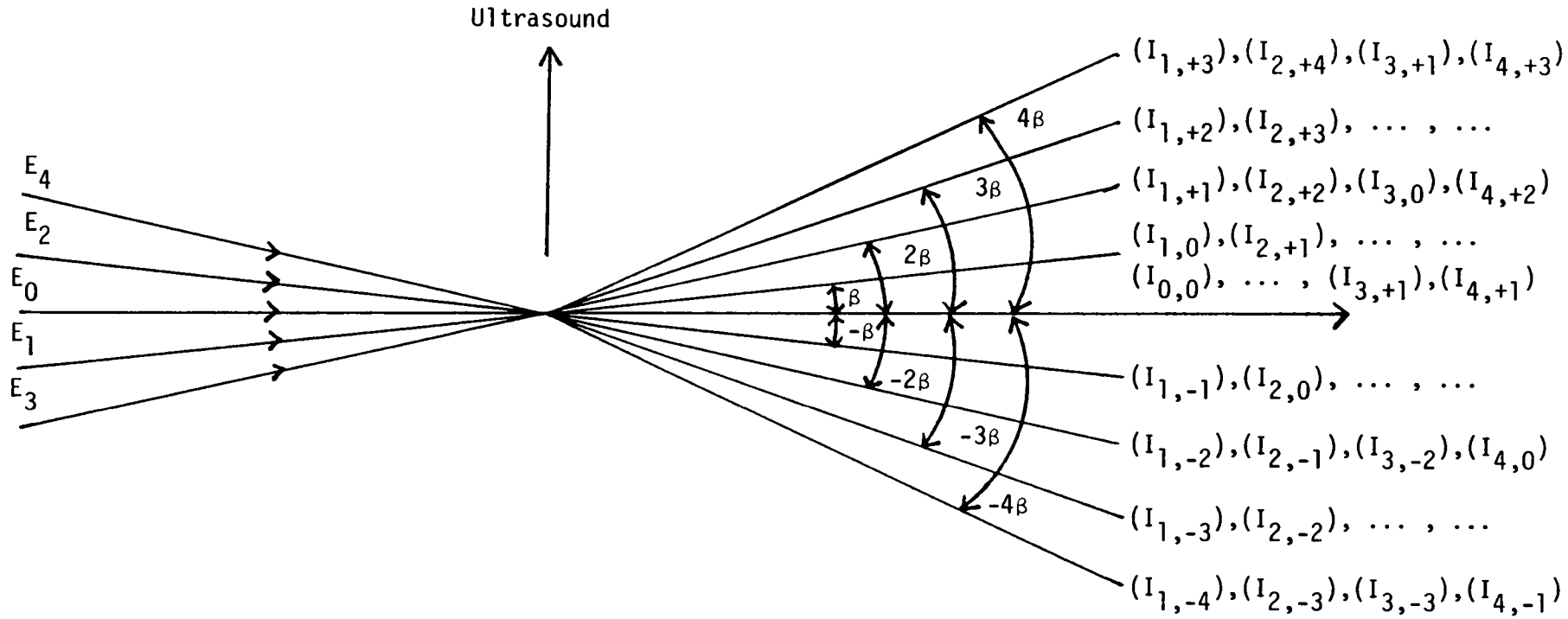


Figure 13. Diagram showing the origin of light arriving at the observed diffraction order.

the constructive interference conditions that give rise to Bragg diffraction. The different directions that are at angles which are an integral multiple of the Bragg angle β may contain light corresponding to all of the components listed. The situation actually turns out to be much simpler than indicated in Figure 13, however. As the theory of Blomme and Leroy shows, many of the diffraction orders in fact contain a negligibility small light intensity. This means that many of the possible components are masked by the more intense components that emerge at the same angle. From this point diffraction orders which are defined theoretically are expressed as "theoretical first diffraction order," "theoretical second diffraction order," etc., while diffraction orders which are defined experimentally; i.e., which are observed on the viewing screen, are expressed as "observed first diffraction order," "observed second diffraction order," etc. This makes it possible to speak meaningfully about a situation that potentially is as confusing as indicated in Figure 13.

I. FIRST-ORDER BRAGG IMAGING

It has been demonstrated experimentally in Chapter III that the observed first diffraction orders contain images of an object in the ultrasonic field and that the images become better as the frequency of ultrasound is increased.

In order to interpret this result Eqs. (72) through (75) are used. Intensities calculated from the theory of Blomme and Leroy with values of parameter ρ which are chosen to match the experimental situation, are shown in Figures 14 and 15 in which the curves are

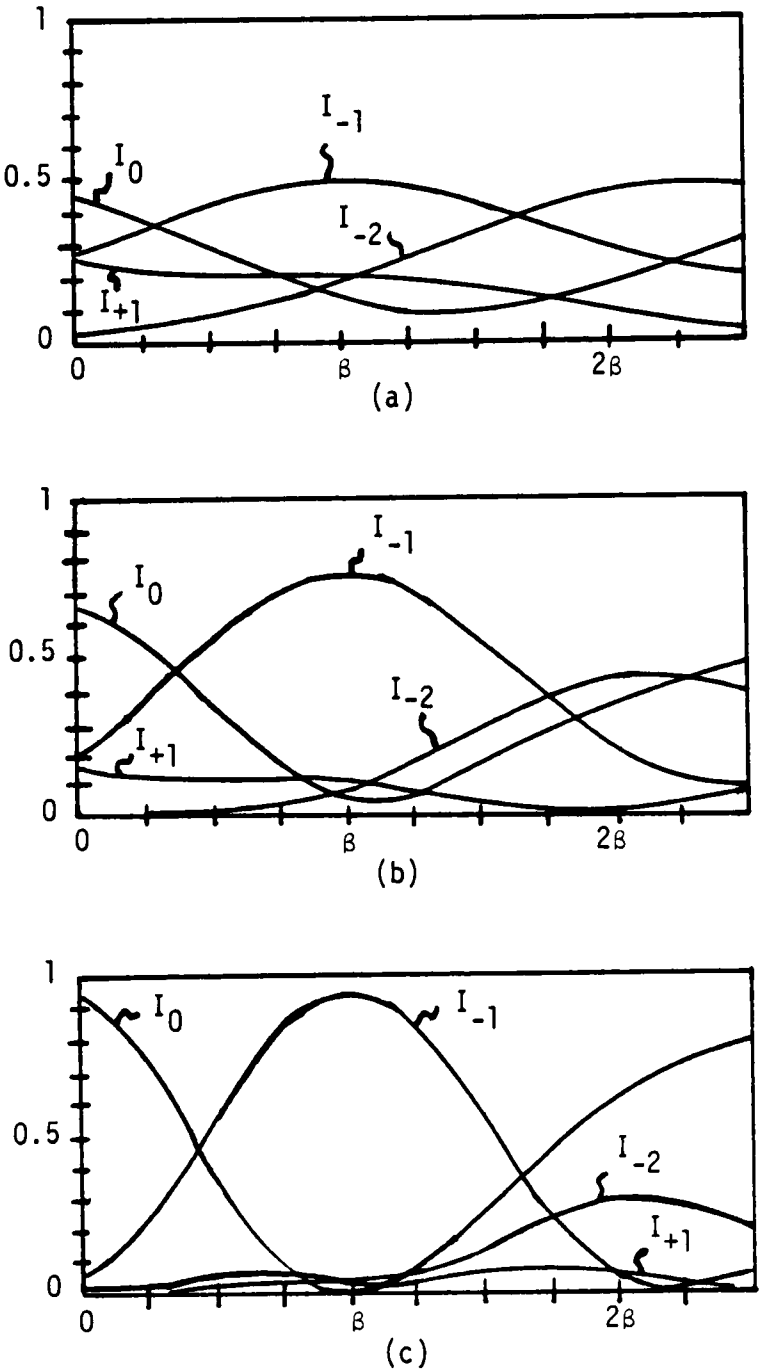


Figure 14. Light intensities plotted as a function of the incident angle of light for $v = 3.09$ ($\mu_1 = 1.3 \times 10^{-5}$) and for (a) $\rho = 1.03$ ($\nu^* = 10$ MHz and $\beta = 5.45$ min); (b) $\rho = 1.48$ ($\nu^* = 12$ MHz and $\beta = 6.54$ min); (c) $\rho = 2.31$ ($\nu^* = 15$ MHz and $\beta = 8.18$ min).

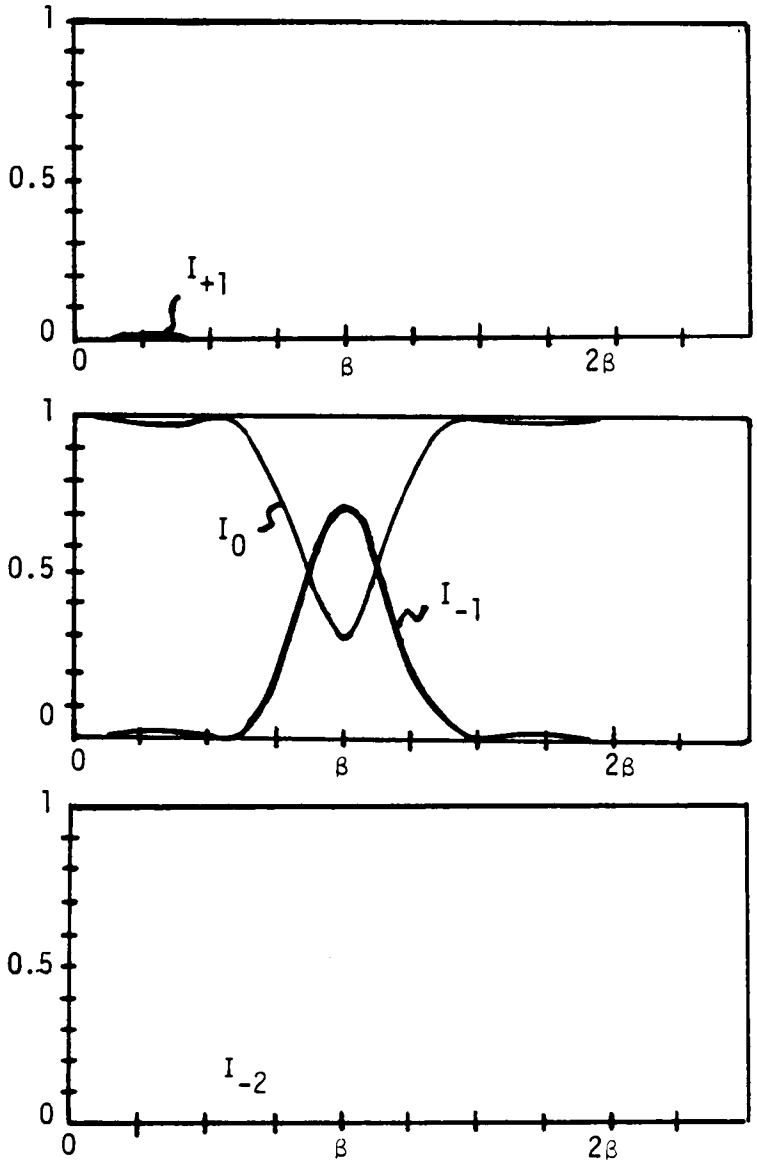


Figure 15. Light intensity plotted as a function of the incident angle of light for $v = 1.43$ and $\rho = 17.48$ ($\nu^* = 28$ MHz and $\beta = 15.27$ min).

plotted as a function of incident angle. The graphs in Figure 14 (a), (b), (c), are obtained with ρ = 1.03 (ν^* = 10 MHz), ρ = 1.48 (ν^* = 12 MHz), and ρ = 2.31 (ν^* = 15 MHz), respectively. Figure 15 is obtained with ρ = 17.48 (ν^* = 28 MHz). The graphs in Figure 15 are shown separately because the diffracted light intensities of the plus first order and the minus second order are not distinguishable if they are shown together with the zero and minus first order.

From Figure 14 one can see that the intensity of the minus first order at incident angle β becomes dominant as the frequency of ultrasound is increased and the intensities of the zero, plus first, and minus second order become lower. This means that the light from these orders becomes less noticeable in the image. In Figure 15 even if the intensity of the minus first order at incident angle β is lower than that of Figure 14(c), the other intensities, i.e., plus first and minus second order, are so low that they are not noticeable. The zero order, however, does contribute to the illumination at the angle β. Since the quality of Bragg imaging in the first order not only depends on the intensity of the minus first order but also depends on the angular width of the minus first order, a higher frequency gives better quality of Bragg imaging in the first order.

II. SECOND-ORDER BRAGG IMAGING

Second-order Bragg imaging has been investigated at frequencies of 6, 10, 12, 15, and 20 MHz. The best second-order images were obtained at the frequency of 12 MHz as shown in Figure 12 (p. 39). This can be explained by the use of Figures 14 and 16.

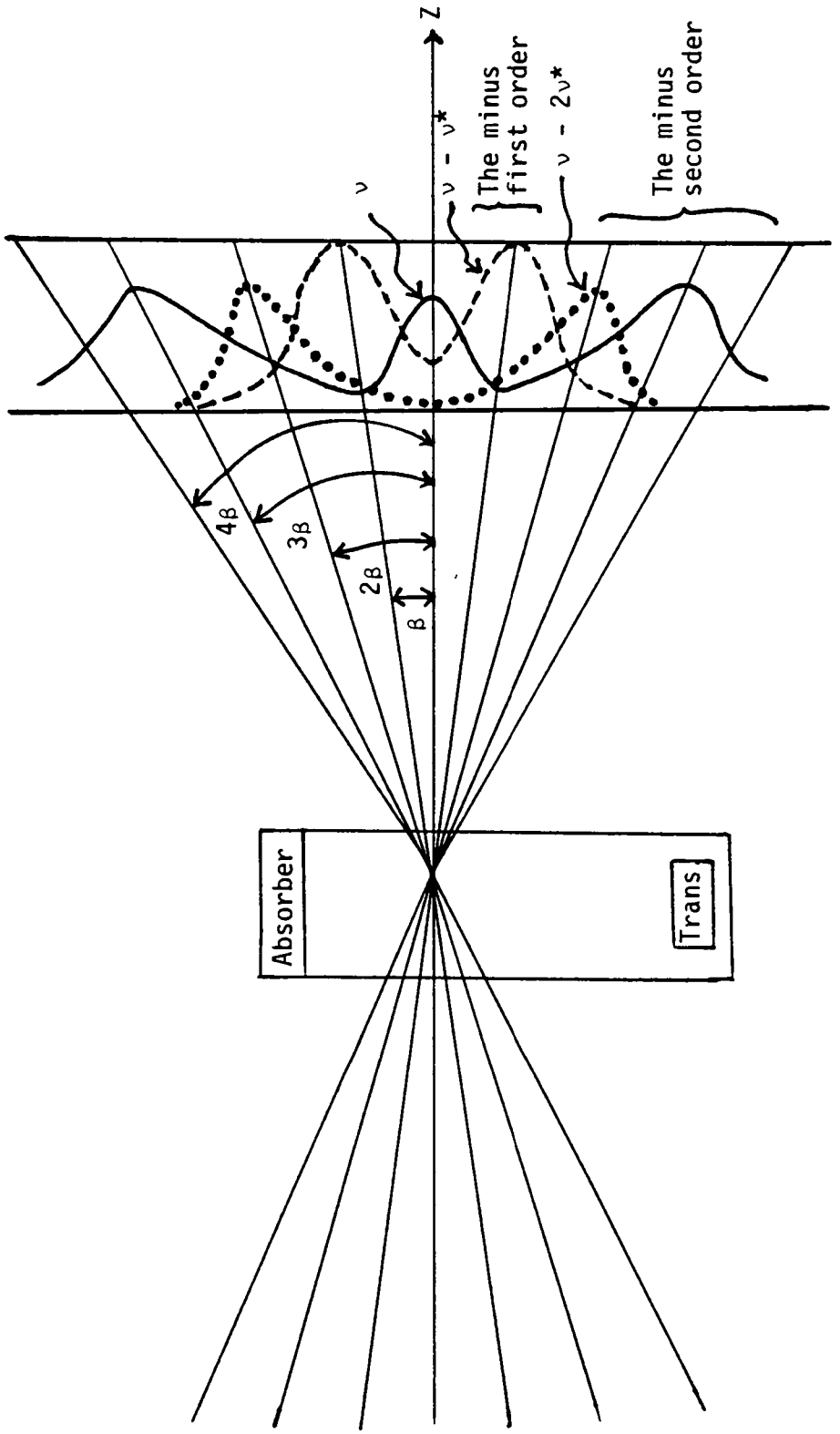


Figure 16. Light intensities of the observed first- and second-order Bragg diffraction corresponding to Figure 14(b).

In Figure 14(b), the second maximum of light intensity of the theoretical zero order appears at about 3β if one extends the curve and the first maximum of light intensity of the theoretical minus second order appears at 2β. These two orders have almost the same intensities at different positions and each order contains its own information about the ultrasonic wavefronts. The intensities of these two orders in Figure 14(a) and (c) are quite different and the positions of the second maxima of light intensities of these orders are not at 2β and 3β. If the angular positions of these maxima are too close, the two images in the observed second order overlap. If they are too far apart, the images are not within the second order. Figure 14(b) is shown more precisely illustrated in Figure 16 in which the intensities of zero, minus first, and minus second order are superimposed. The unbroken, broken, and dotted line in Figure 16 represents theoretical zero, first, and second order, respectively. The observed minus first order is composed of the intensity of the theoretical minus first order and the observed minus second order is composed of the intensities of the theoretical zero and minus second order. From this result one can see that there exist two images in the second order because two different theoretical orders contribute to making the observed second order.

The qualities of two images in the observed second order are not the same when the frequencies of ultrasound are 10 MHz and 15 MHz. From Figures 14(a) and (c) the intensities of the theoretical zero and

minus second order which contribute to making the observed minus second order are quite different, which explains the difference in image quality.

CHAPTER V

APPLICATION OF BRAGG IMAGING TO FLAW DETECTING

A unique application of Bragg imaging to flaw detection has been developed during the course of the research. The technique takes advantage of the resonance behavior of a parallel metal plate immersed in a liquid. Excitation of the plate by an ultrasonic beam results in strong transmission of the ultrasound for angles of incidence which set up Lamb mode resonances in the plate. Such a plate with an internal flaw does not transmit the ultrasound through the flaw. The result is an image of the flaw in the transmitted ultrasonic wavefront. The ability of Bragg diffraction to image ultrasonic wavefronts makes it ideal for decoding the information contained in the ultrasonic wavefront.

The principle can be illustrated by use of a 1.1 mm thick plate of glass mounted in front of a 4 MHz square quartz transducer. First the transducer is aligned to give optimum Bragg diffraction. Then the glass plate is inserted between the transducer and the light beam and rotated until optimum Bragg diffraction again is observed. The experimental situation is shown in Figure 17. The angle of rotation of the plate for optimum transmission of the ultrasound is approximately 7° at 4 MHz. The glass plate used in the experiment had the symbol Ⅎ scratched on its surface as shown in Figure 18(a). The plate is mounted between the transducer and light beam and rotated to give optimum transmission with 20 MHz of frequency. When the plate is adjusted so that the symbol is in the ultrasonic beam, the first

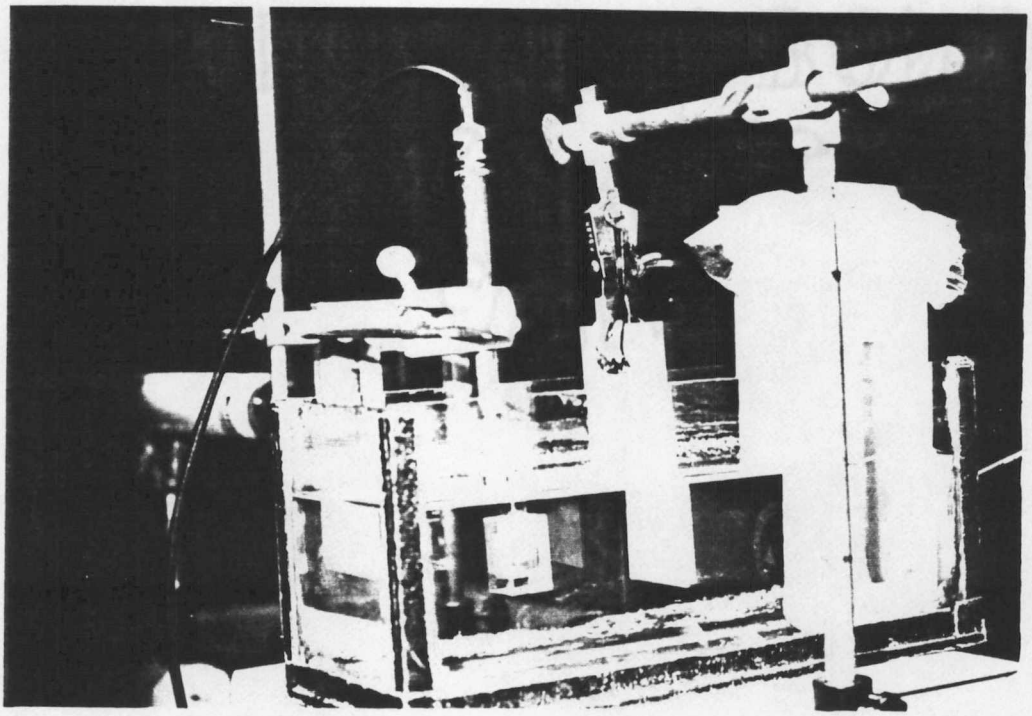
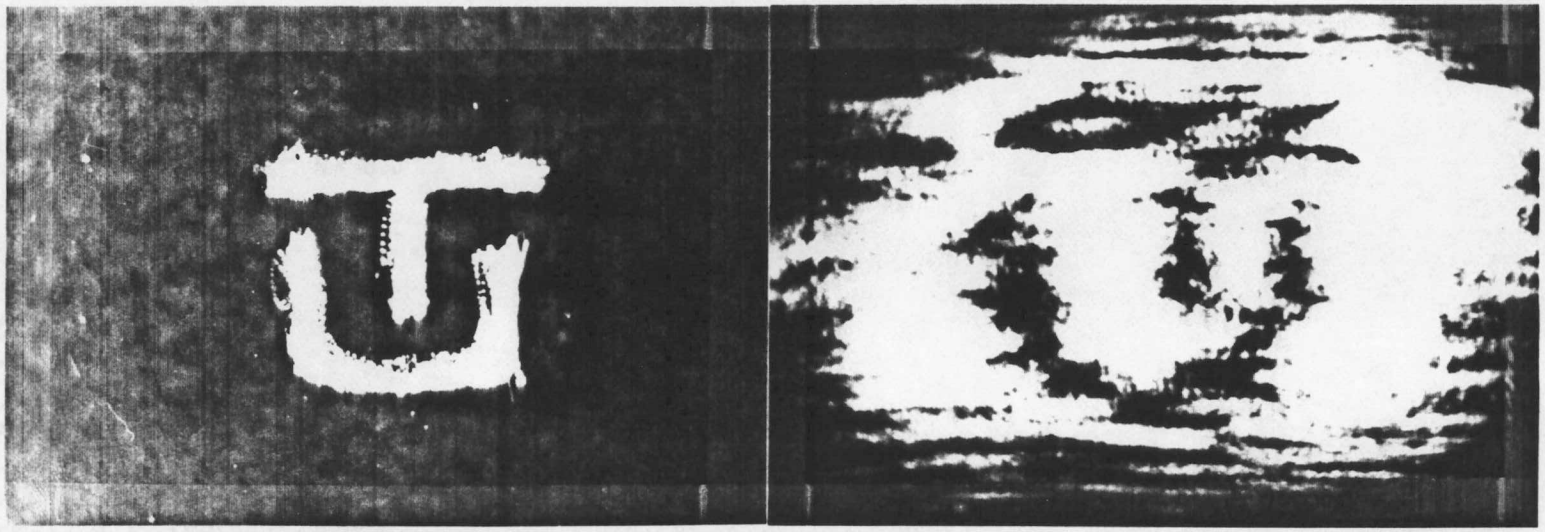


Figure 17. Photograph of experimental arrangement for flaw detecting.



(a) (b)

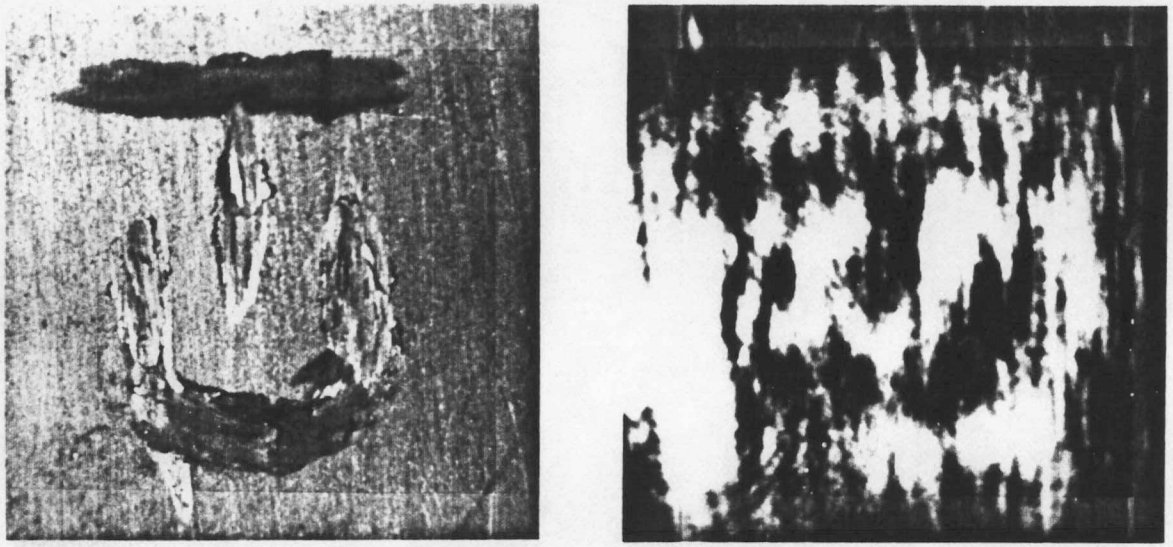
Figure 18. Photographs of the symbol Ш on the glass plate and its image, frequency 20 MHz.

diffraction order appears as shown in Figure 18(b). The symbol appears as a dark line because the intensity of the transmitted ultrasonic wave at the symbol is very low, and essentially no Bragg diffraction occurs in this region. Some of the angles of rotation of the plate for transmission maxima at 12 MHz are shown in Table II.

The principle illustrated now can be used to image a flaw that is obscured from view. An aluminum plate, thickness 1.6 mm, is used in the same way, except that now a second aluminum plate, thickness 1.6 mm, is clamped so that it obscures the symbol. With the same symbol ⫪ scratched on the inside surface of the first plate, the plates are inserted into a 20 MHz ultrasonic beam. Figure 19 shows that the obscured symbol is recognizable in the diffraction order. In this figure a small scratch on the lower left corner of the symbol is also recognizable in the image. This means that a fair amount of detail can be discerned in the image. In fact, moving the image back and forth aids in visualizing image details. The same experiment has been done with two other aluminum plates, thickness 0.9 mm each, to test the resolution of the technique. Two letters, A and F, are scratched on the surface of one of them. The letters on the plate and their images are shown in Figure 20. In this case the image of F is not as clear as the image of A; however, the general shape of both letters can be visualized. Finally, although Figures 18, 19, and 20 show that Bragg diffraction allows one to visualize internal structures in plates, further testing will be necessary not only to define resolution limits but also to determine the optimum procedure for locating a flaw in a given situation.

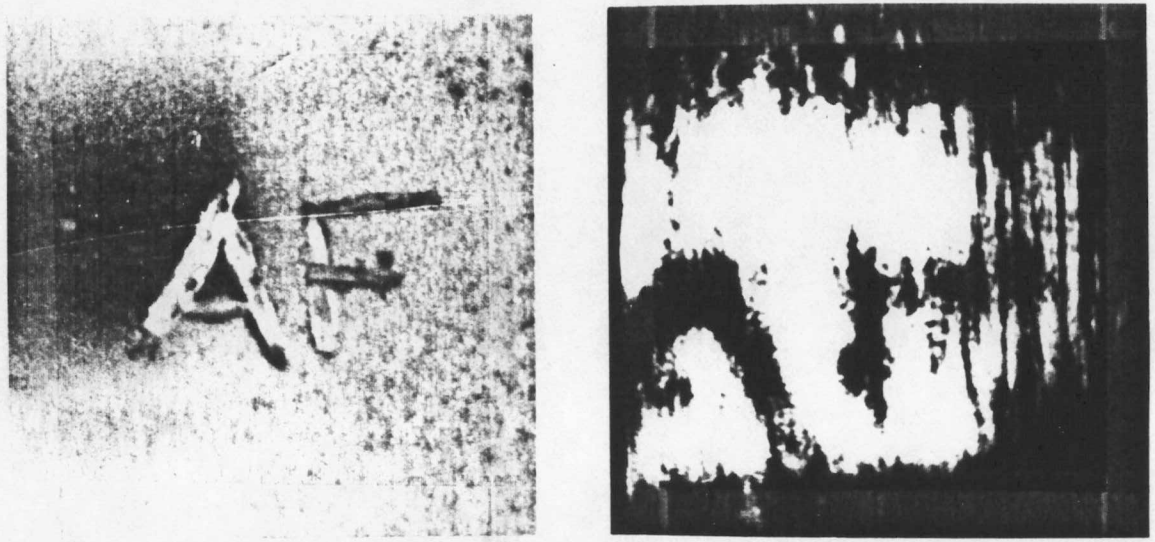
Table II. Angles At Which Optimum Bragg Diffraction is Observed With a Glass Plate 1.1 mm Thick, Frequency 12 MHz

Angle (°)			
α_1		5.3	First Maximum to Clockwise
α_2	$\alpha_1 + 4.6$	9.9	Second
α_3	$\alpha_2 + 3.3$	13.2	Third
α_4	$\alpha_3 + 2.2$	15.4	Fourth
α_5	$\alpha_4 + 3.2$	18.6	Fifth
α_6	$\alpha_5 + 2.7$	21.3	Sixth
α_{-1}		5.3	First Maximum to Counter-clockwise
α_{-2}	$\alpha_{-1} + 4.6$	9.9	Second
α_{-3}	$\alpha_{-2} + 2.9$	12.8	Third
α_{-4}	$\alpha_{-3} + 2.6$	15.4	Fourth
α_{-5}	$\alpha_{-4} + 3.0$	18.4	Fifth
α_{-6}	$\alpha_{-5} + 2.9$	21.3	Sixth



(a) (b)

Figure 19. Photographs of the symbol Ψ on the aluminum plate and its image, frequency 20 MHz.



(a) (b)

Figure 20. Photographs of the letters A and F scratched on the surface of an aluminum plate and their images.

CHAPTER VI

SUMMARY, CONCLUSIONS, AND SUGGESTIONS FOR FURTHER WORK

I. SUMMARY AND CONCLUSIONS

Bragg diffraction of light by ultrasonic waves has been studied between 4 MHz and 28 MHz. At the low frequencies the diffraction exhibits both the Bragg diffraction character and the character of Raman-Nath diffraction. As the frequency is increased Bragg diffraction becomes more dominant and imaging of the ultrasonic wavefront in the diffraction order is observed. The transition from Raman-Nath diffraction to Bragg diffraction is conveniently described by the quantity Q of Klein, Cook, and Mayer. Values of Q smaller than 1 signify that the diffraction is predominantly of the Raman-Nath type. Values greater than 10 correspond to Bragg diffraction. The highest values of Q correspond to total Bragg diffraction. This is where Bragg imaging is best.

Optimum conditions for Bragg diffraction have been defined by the graphs in Figures 14 and 15 (pp. 43 and 44) which show that Bragg diffraction and the associated Bragg imaging is better and better as the frequency is increased up to the practical limit set by attenuation which also increases with frequency. For water as a propagating medium this limit is near the maximum frequency used in the experiments described—28 MHz.

Single images of the ultrasonic wavefront were observed in the first diffraction orders. They are mirror images in the positive and negative orders. Multiple images are observed in the higher diffraction orders. The existence of two images in the second orders was found to be related to the fact that conditions for diffracted light's arriving at the position of the second order can be satisfied for light incident at 3β as well as for light incident at 2β. The best images in the second orders were obtained at 12 MHz. This intermediate frequency gives the maximum concentration of light in the second order, as is noted in the graphs in Figure 14 (p. 43).

Finally, it is shown in this thesis that Bragg imaging of an ultrasonic wavefront can be used to detect flaws inside glass or metal plates. For incident angles at which Lamb modes are set up in parallel plates there is a maximum in the transmitted ultrasonic energy. At these angles interval flaws in the plate inhibit the passage of the ultrasonic energy, and hence are imaged as shadows on the ultrasonic wavefront. The fact that Bragg diffraction images the wavefront means that the flaw is seen in the Bragg diffraction order as well.

II. SUGGESTIONS FOR FURTHER WORK

The graphical approach used in this thesis to explain the existence of two images in the second order could be extended to describe even higher order images. To do so the NOA method of Blomme and Leroy would need to be extended to higher orders and the experiment would need to be done with a larger angular spread of the convergent incident light.

It may be possible to improve the quality of the image of a flaw inside a parallel plate by using a medium having a lower ultrasonic wave velocity than water. One possibility would be carbontetrachloride. The shorter wavelength associated with the lower velocity would result in better resolution. With such a system one might consider imaging delaminations on printed circuit boards. Such delaminations are difficult to detect by other means.

It is conceivable that flaws could be detected in more than a single plate. In principle the technique would work with multiple layers of liquid and solid. Hence any number of layers might be examined.

BIBLIOGRAPHY

BIBLIOGRAPHY

Blomme, E. and O. Leroy, Acustica 59, 182-192 (1986).

Klein, W. R., B. D. Cook, and W. G. Mayer, Acustica 15, 67-74 (1965).

Klein, W. R. and B. D. Cook, IEEE SU14, 123-134 (1967).

Korpel, A., Optical Imaging of Ultrasonic Fields by Acoustic Bragg Diffraction (Rotterdam, 1969).

Leroy, O. and E. Blomme, Ultrasonics, 125-131 (1984).

Martin, F. D., Ph.D. Dissertation (University of Tennessee, Knoxville, 1971).

Nath, N. S. N., Proc. Indian Acad. Sci. 4, 262-274 (1936).

Phariseau, P., Proc. Indian Acad. Sci. 44, 165 (1956).

Pitts, L. E., T. J. Plona, and W. G. Mayer, J. Acoust. Soc. Am. 60, 374-377 (1976).

Raman, C. V. and N. S. N. Nath, Proc. Indian Acad. Sci. 2, 406 (1935).

Raman, C. V. and N. S. N. Nath, Proc. Indian Acad. Sci. 2, 413 (1935).

Raman, C. V. and N. S. N. Nath, Proc. Indian Acad. Sci. 3, 75 (1936).

Raman, C. V. and N. S. N. Nath, Proc. Indian Acad. Sci. 3, 119 (1936).

Raman, C. V. and N. S. N. Nath, Proc. Indian Acad. Sci. 3A, 459 (1936).

Raman, C. V. and K. S. Venkaterman, Proc. Roy. Soc. (London), 171, 137-147 (1939).

VITA

Jeong K. Na was born in Busan, Korea, on November 21, 1959. He graduated from Busan-Jin High School in 1978. In 1982, he received his Bachelor of Science degree in physics from Dong-A University, Busan, Korea. The following spring he began study toward a Master of Science degree in physics at Dong-A University. In February 1983 he accepted a graduate teaching assistantship and completed the Master of Science degree in 1984.

He came to The University of Tennessee, Knoxville, in September 1984. In September 1985 he was granted a Research Assistantship under sponsorship of the Office of Naval Research. He was awarded the Master of Science degree in December 1986 from The University of Tennessee, Knoxville.

He was married to the former Il Cheon in 1984. They have one daughter, In Ja, age 1.